



## OPEN ACCESS

## EDITED BY

Peter David Roopnarine,  
California Academy of Sciences, United States

## REVIEWED BY

Jaelyn J. Eberle,  
University of Colorado Boulder, United States  
Douaa Fathy,  
Minia University, Egypt

## \*CORRESPONDENCE

M. B. Suarez,  
✉ mb.suarez@ku.edu

RECEIVED 04 October 2024

ACCEPTED 15 April 2025

PUBLISHED 13 May 2025

## CITATION

Allen ML, Suarez MB, Adams TL and Suarez CA  
(2025) Ecohydrology and paleoenvironment  
of the Cretaceous (Albian) Cloverly  
Formation: insights from multi-taxon oxygen  
isotope analysis of vertebrate phosphates.  
*Front. Earth Sci.* 13:1497416.  
doi: 10.3389/feart.2025.1497416

## COPYRIGHT

© 2025 Allen, Suarez, Adams and Suarez. This  
is an open-access article distributed under  
the terms of the [Creative Commons  
Attribution License \(CC BY\)](#). The use,  
distribution or reproduction in other forums is  
permitted, provided the original author(s) and  
the copyright owner(s) are credited and that  
the original publication in this journal is cited,  
in accordance with accepted academic  
practice. No use, distribution or reproduction  
is permitted which does not comply with  
these terms.

# Ecohydrology and paleoenvironment of the Cretaceous (Albian) Cloverly Formation: insights from multi-taxon oxygen isotope analysis of vertebrate phosphates

M. L. Allen<sup>1</sup>, M. B. Suarez<sup>2\*</sup>, T. L. Adams<sup>3</sup> and C. A. Suarez<sup>4</sup>

<sup>1</sup>Department of Earth and Environmental Sciences, University of Michigan, Ann Arbor, MI, United States, <sup>2</sup>Department of Geology, University of Kansas, Lawrence, KS, United States, <sup>3</sup>Witte Museum, San Antonio, TX, United States, <sup>4</sup>Department of Geosciences, Fayetteville, AR, United States

The Cloverly Formation of Montana and Wyoming preserves abundant nonmarine vertebrate fossils from the mid-Cretaceous, yet its paleoenvironment and faunal niche structure remain poorly understood. We analyzed  $\delta^{18}\text{O}_{\text{phosphate}}$  in over 100 fossil individuals from multiple vertebrate taxa collected from a single microfossil bonebed in Carbon County, Montana. To infer habitat preferences and water-use strategies, we compared  $\delta^{18}\text{O}_{\text{phosphate}}$  values within and across taxa. We reconstructed  $\delta^{18}\text{O}_{\text{surface\_water}}$  from semi-aquatic reptile values using regressions calibrated with data from modern environments and extant taxa. Using a multi-taxon framework, we estimated warm-season water temperatures from  $\delta^{18}\text{O}_{\text{surface\_water}}$  and  $\delta^{18}\text{O}_{\text{phosphate}}$  of lepisosteid (gar) scales, then converted these to air temperatures using a modern climate transfer function.  $\delta^{18}\text{O}_{\text{phosphate}}$  values ranged from 9.5‰ to 23.2‰ (VSMOW) and varied across taxa. Aquatic and semi-aquatic groups exhibited lower values than dinosaurian taxa. Our reconstructed mean  $\delta^{18}\text{O}_{\text{surface\_water}}$  was  $-7.9\text{‰}$  (95% CI:  $-10.1$  to  $5.5\text{‰}$ ), yielding a warm-season water temperature of  $26^{\circ}\text{C}$  and an air temperature of  $24^{\circ}\text{C}$ . Intertaxon differences reflect niche partitioning and suggest primary isotopic signals are preserved. Unexpectedly high values in Bernissartiid-like neosuchian teeth may indicate greater ecohydrological diversity than previously recognized. Our  $\delta^{18}\text{O}_{\text{surface\_water}}$  estimate aligns with other Aptian-Albian proxies but exceeds model-based predictions, likely due to outdated assumptions underlying the model. The MAWSAT estimate falls within the upper range of model-data assimilation outputs. These results provide new context for ecological structure in the Cloverly fauna and offer the first quantitative temperature estimate for the Formation, helping to define baseline conditions between the Aptian-Albian Cold Snap and the Cretaceous Thermal Maximum.

## KEYWORDS

mid-Cretaceous, Aptian-Albian, terrestrial paleoclimate, vertebrate paleoecology, Cloverly Formation, stable oxygen isotopes

## 1 Introduction

The nonmarine Cloverly Formation of Wyoming and Montana is well known for its classic dinosaurian fauna and has been the subject of intense paleontological interest for nearly a century. The Cloverly fauna is one of several Early Cretaceous assemblages that offer a window into macroevolutionary and biogeographic change in North American nonmarine systems between the better-sampled Late Jurassic and Late Cretaceous. Microvertebrate sampling campaigns over the last few decades have significantly improved our understanding of the Cloverly vertebrate fauna. Still, little is known about the paleobiology and paleoenvironment of the Cloverly vertebrates. Our current knowledge of Cloverly vertebrate ecology is based on morphology and histology alone, and our understanding of the local environments is based almost exclusively on inferences from faunal composition and sedimentology. Cloverly ecosystems can be improved by including isotopic evidence from fossils and geological materials. Stable oxygen isotopes from Cretaceous nonmarine vertebrate fossils have been shown to preserve information about biotic factors such as habitat resource partitioning, biological water use, and physiology, as well as abiotic factors such as surface air temperatures and regional hydroclimate (Amiot et al., 2006; Amiot et al., 2010; Amiot et al., 2011; Suarez et al., 2011; Suarez et al., 2012; Pouech et al., 2014; Suarez et al., 2014; Amiot et al., 2015; Cullen et al., 2020; Amiot et al., 2021; Cullen et al., 2022). We measured  $\delta^{18}\text{O}_{\text{phosphate}}$  (abbreviated as  $\delta^{18}\text{O}_{\text{p}}$ ) from a wide array of vertebrate groups from a single Cloverly microfossil vertebrate bonebed in southeastern Montana. This assemblage (Oklahoma Museum of Natural History site V1075) is an ideal target for a broad scale multi-taxon  $\delta^{18}\text{O}$  study because it is exceptionally rich and taxonomically diverse for a Cloverly assemblage. Analyzing multiple specimens from multiple ecomorphological groups in a single bonebed allows us to evaluate the fractionation of oxygen isotopes across the ecological landscape over a relatively short amount of geologic time.

During the Late Jurassic and Early Cretaceous, the Western Interior Basin (WIB) formed as a retroarc foreland basin resulting from flexure driven by convergence at the Sevier Thrust Belt to the west (Heller and Paola, 1988; DeCelles, 2004; D'Emic et al., 2019). From the Late Jurassic throughout much of the Early Cretaceous, deposition in the basin was dominated by alluvial plains. Eustatic sea level rise and increased subsidence in the WIB resulted in epeiric flooding of much of the basin by the mid to late Albian. Upper Cloverly Formation deposits represent a coastal plain environment, with the Sevier Mountains nearby to the west and the incipient Western Interior Seaway nearby to the east (Figure 1). In general, the Cretaceous was predominantly a period of greenhouse conditions (Scotese et al., 2025; Judd et al., 2024; Huber et al., 2018). Evidence suggests, however, that there may have been at least one interval of cooler or even icehouse conditions spanning the Aptian-Albian transition (McAnena et al., 2013; Rodríguez-López et al., 2016; Harper et al., 2021). This "Aptian-Albian Cold Snap" was shortly followed by dramatic warming culminating in one of the hottest periods in the Phanerozoic, the Cretaceous Thermal Maximum (Huber et al., 2018; Jones et al., 2022). These global patterns, combined with regional geographic evolution, further complicated climatic change in the Western Interior during this time. As the Sevier Orogeny continued its uplift

to the west, a rain shadow developed across parts of the region (Suarez et al., 2014; Ludvigson et al., 2015). These arid conditions gave way to humid conditions as regional subsidence and eustatic sea level rise allowed the Western Interior Sea to encroach on the Cloverly region, supplying moisture to the local atmosphere.

The stratigraphy of the Cloverly Formation is highly complex, varying from site to site even within the Bighorn Basin (Moberly, 1960; Ostrom, 1970; D'Emic et al., 2019). Still, there are some general patterns that seem to be consistent across much of the Basin. The lowermost Cloverly is often characterized by the presence of conglomeratic sandstones representing an east-flowing series of braided river plains that developed during a pulse in increased uplift of the Sevier Orogeny. These deposits are often referred to as the Pryor Conglomerate Member. As uplift and deposition slowed, Cloverly deposition became dominated by fluvial floodplains with low sedimentation rates and extensive pedogenesis (Elliott et al., 2007). The interval overlying the Pryor Conglomerate is mostly comprised of bentonitic mudstones with abundant carbonate nodules and limestone beds, although gleyed floodplain paleosols with little to no carbonate are also present. This interval is typically referred to as the Little Sheep Mudstone Member. The Himes Member overlies the Little Sheep Mudstone, although the two members can be difficult to distinguish in some cases. The Himes is similar to the Little Sheep but generally contains less evaporative facies, and the upper interval of the Himes is often comprised of gleyed floodplain paleosols. Overlying the Himes Member are the marginal marine deposits of the Sykes Mountain Formation, which indicate the local arrival of the Western Interior Seaway.

Most bonebeds in the Cloverly primarily yield macrofossil assemblages dominated by large dinosaur taxa. These assemblages are typically low in richness. Common taxa from these sites include the iguanodontid ornithomorph *Tenontosaurus tilletti*, the basal dromaeosaurid *Deinonychus antirrhopus*, the nodosaurid ankylosaur *Sauropelta edwardsi*, the allosauroid theropod *Acrocanthosaurus sp.*, and the titanosaur sauropod *Sauroposeiden sp.* Common non-dinosaurian macrofossil taxa include crocodylomorphs and turtles, as well as ceratodontid and amioid fishes. Microfossils are present at some of these classic sites but are not abundant or diverse. Over the last few decades, however, prolific vertebrate microfossil bonebeds have been discovered in the northern Bighorn Basin in southeastern Montana (Oreska et al., 2013). These microfossil assemblages have more than doubled the known vertebrate diversity of the Cloverly. These sites have yielded tyrannosauroids, amphibians, lepidosaurs, chondrichthyans, and juvenile dinosaurs, as well as trechnotherian, eutriconodontid, multituberculata, and symmetrodontid mammals (Jenkins and Schaff, 1988; Maxwell and Horner, 1994; Cifelli et al., 1998; Cifelli, 1999; Gardner, 1999; Nydam and Cifelli, 2002; Oreska et al., 2013).

Oxygen isotopes from vertebrate fossils are particularly useful as paleoecological proxies because they can inform on both abiotic and biotic parameters (Kohn and Cerling, 2002; Koch, 2007; Suarez et al., 2014). The  $\delta^{18}\text{O}$  of vertebrate bioapatite is determined by  $\delta^{18}\text{O}_{\text{body\_water}}$ , body temperature, and a kinetic fractionation phenomenon associated with biomineralization often referred to as the "vital effect." When the vital effect and body temperature are quantitatively constrained,  $\delta^{18}\text{O}_{\text{body\_water}}$  can be estimated.  $\delta^{18}\text{O}_{\text{body\_water}}$  of vertebrates can then be used to make inferences about environmental and biological parameters such

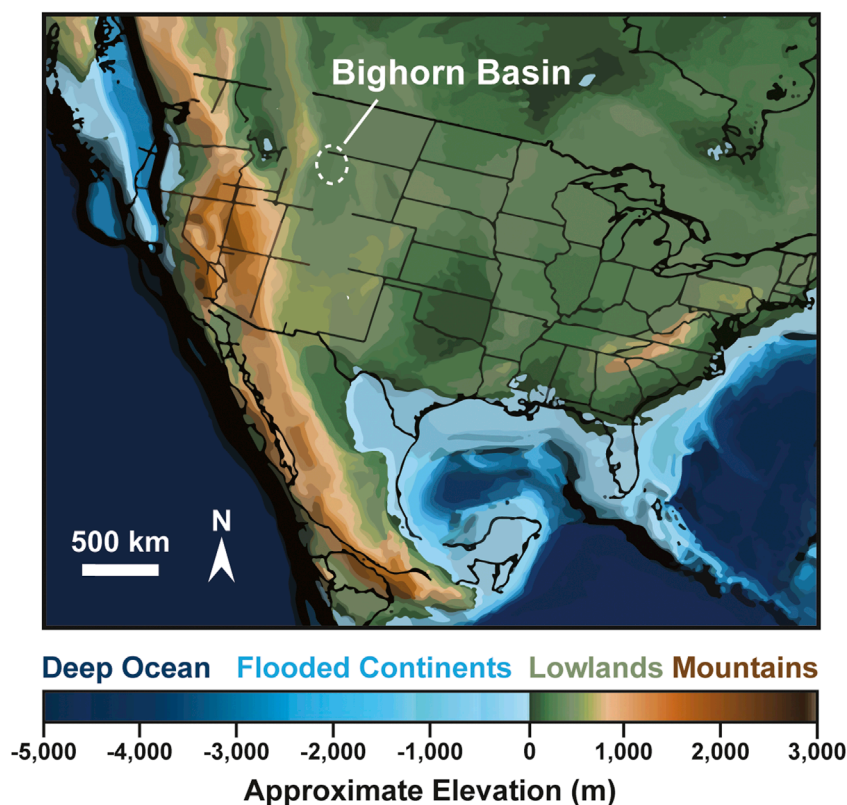


FIGURE 1

Paleogeographic reconstruction of North America (modified from, [Scotese, 2021](#)) during the mid Albian (110 Ma) showing the location of the Cloverly Formation. Map is a rectilinear projection with approximate overlain US state outlines. The Cloverly was deposited in a foreland sub-basin during the Albian. By the Late Albian, the Western Interior Seaway had flooded the axis of the Western Interior Basin, encroaching on the Cloverly region. The Sevier Mountains were likely less than 100 km to the west. The Cloverly was deposited on fluvial plains with very shallow topographic gradients.

as the  $\delta^{18}\text{O}$  of ingested waters and an animal's water economy.  $\delta^{18}\text{O}$  of ingested water depends on the  $\delta^{18}\text{O}$  of precipitation and hydroclimatic factors such as environmental water stress, seasonality of precipitation, and regional moisture sources. Biotic controls on  $\delta^{18}\text{O}$  of body water include physiology, thermoregulatory behavior, habitat preference, and diet. The oxygen isotope composition of vertebrate body water can be inferred from  $\delta^{18}\text{O}$  of either the carbonate or phosphate fraction of biogenic hydroxyapatite. However, the phosphate fraction is less susceptible to diagenetic overprinting of primary isotope signals due to the relatively strong bond between phosphorous and oxygen in phosphate ([Kolodny et al., 1983](#); [Kohn and Cerling, 2002](#); [Lee-Thorp, 2002](#)). Adversely, the bond between carbon and oxygen in carbonate is weaker and is more susceptible to the replacement of oxygen atoms in the molecular structure. Also, in typical bioapatite, phosphate-bound oxygen is about ~35% by mass, as opposed to only about 3.3% for carbonate-bound oxygen ([Cerling and Sharp, 1996](#)). This means that far less fossil sample material is required for mass spectrometry of phosphates than for carbonates. The availability of any given fossil taxon at a particular site is often limited. Although bone material is often plentiful, given the small amount of powder needed for each sample (300–600  $\mu\text{g}$ ), tooth enamel is preferred as it is more resistant to diagenetic overprinting than bone or dentine ([Kohn and Cerling, 2002](#)). Tooth enamel in many taxa is very thin, limiting the

amount of available sample material. Also, many teeth in Cretaceous nonmarine fossil assemblages are quite small, further limiting the amount of sampleable material available. Acquiring an adequate amount of carbonate sample from tooth enamel in many of the taxa of the Cloverly Formation would require destruction of the entire tooth surface.

Few ecosystem-scale isotopic studies have focused on terrestrial vertebrate faunas from the mid-Cretaceous of North America. In contrast, several studies have examined  $\delta^{18}\text{O}$  values across multiple sympatric taxa from the earliest and mid-Cretaceous in East Asia, France, South Africa, and Brazil ([Amiot et al., 2021](#); [Amiot et al., 2015](#); [Amiot et al., 2011](#); [Amiot et al., 2010](#); [Amiot et al., 2009](#)). In North America, [Suarez et al. \(2014\)](#) conducted an isotopic study of vertebrates from the Aptian and Cenomanian of Utah. These studies have provided valuable insights into paleoenvironmental conditions as well as isotopic niche structures in mid-Cretaceous terrestrial systems. However, the isotopic distribution in and between terrestrial vertebrate groups from other mid-Cretaceous deposits of North America is lacking, limiting our ability to interpret how these ecosystems responded to the significant environmental changes over space and time. This knowledge gap complicates the application of isotopic proxies derived from vertebrate bioapatite in this region. To address this, we present the first ecosystem-scale  $\delta^{18}\text{O}$  analysis of a vertebrate fauna from the Cloverly Formation. This high-resolution

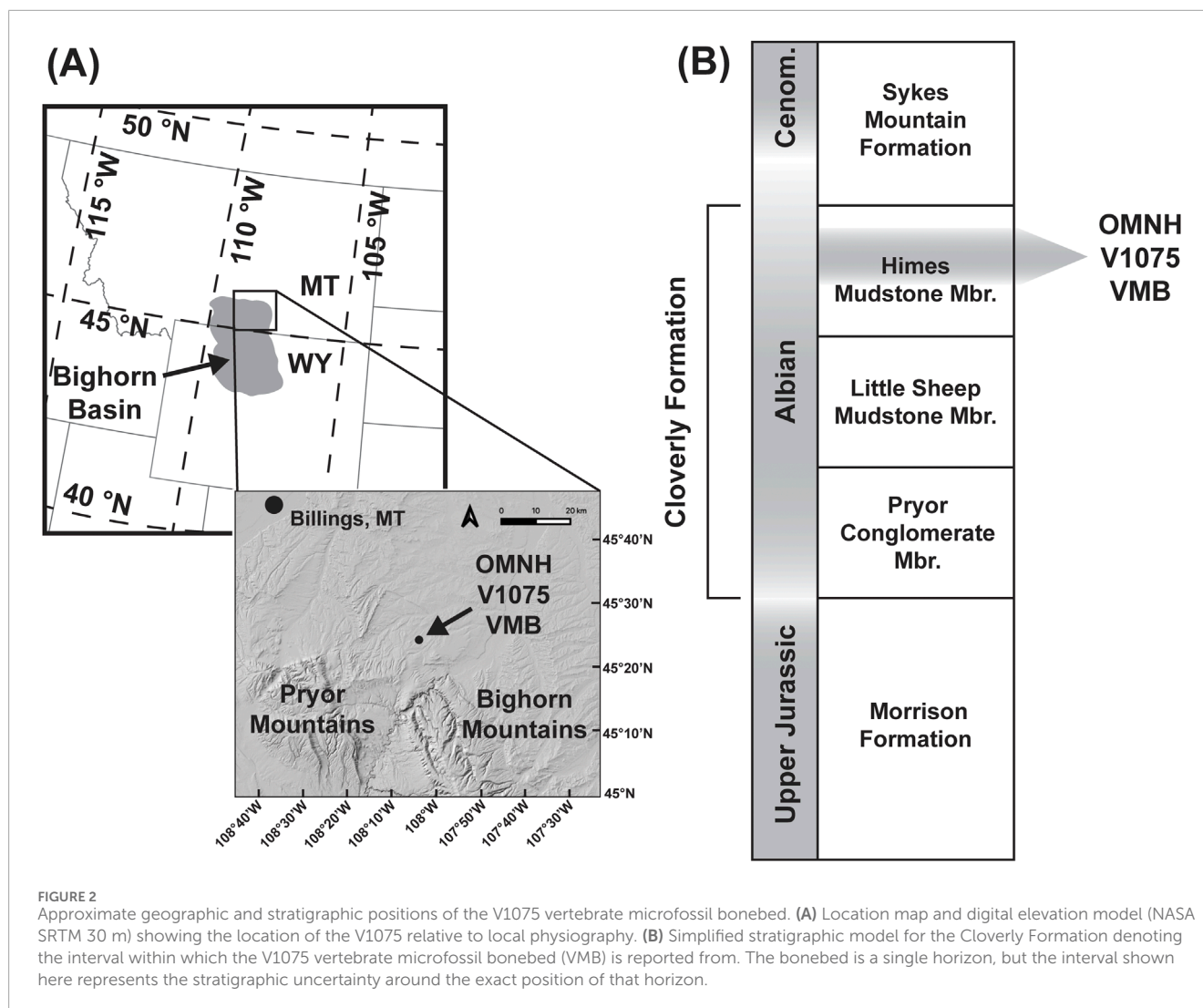


FIGURE 2

Approximate geographic and stratigraphic positions of the V1075 vertebrate microfossil bonebed. (A) Location map and digital elevation model (NASA SRTM 30 m) showing the location of the V1075 relative to local physiography. (B) Simplified stratigraphic model for the Cloverly Formation denoting the interval within which the V1075 vertebrate microfossil bonebed (VMB) is reported from. The bonebed is a single horizon, but the interval shown here represents the stratigraphic uncertainty around the exact position of that horizon.

dataset provides a foundation for developing a framework to interpret smaller  $\delta^{18}\text{O}$  datasets from mid-Cretaceous terrestrial vertebrate fossil assemblages in North America and elsewhere.

## 2 Materials and methods

### 2.1 Materials, sampling, and stable isotope analysis

Teeth, scales, and turtle shell fragments from a single locality (V1075) in Bighorn County, Montana were approved for consumptive sampling from the Oklahoma Museum of Natural History (OMNH). The geographic location and stratigraphic position of the V1075 bonebed is shown in Figure 2. Detailed locality data is available from the OMNH upon request. The V1075 site has yielded an abundant and taxonomically rich vertebrate microfossil assemblage, especially in comparison to other OMNH Cloverly sites. Museum records claim that the assemblage was collected by bulk screenwashing from near the base of Ostrom's "Unit VII" but the precise stratigraphic position is unknown.

Although there are no direct age constraints at the V1075 site, recent radiometric dates from multiple sites across the Bighorn Basin have constrained the depositional age of the Cloverly to the Albian stage (Carrano et al., 2022; D'Emic et al., 2019). Recent work has provided high-precision U/Pb dates from cryptotephra zircons collected at multiple points in a section near Crooked Creek, approximately 50 km south-southeast of the V1075 site (J. Fekete, pers. Comm., December 2024). These Crooked Creek dates have further constrained the Little Sheep-Himes boundary interval to ~110–109 Ma. The V1075 fauna is typical of the Cloverly, having tooth morphotypes sharing affinities with *Deinonychus* and *Tenontosaurus*. The dinosaur fauna also includes sauropods, carcharodontosaurids, troodontids, and nodosaurids. Neosuchian crocodylomorph teeth are especially abundant, including thousands of specimens of tooth morphotypes sharing affinities with goniopholidids, atoposaurids, bernissartiids, and pholidosaurs. Family-level designations of crocodylomorph teeth from the Cloverly are tenuous due to the lack of described macrofossils. We sampled all four of the present neosuchian tooth morphotypes. However, the pholidosaur-like teeth were small and had thin enamel, making recovery of viable sample sizes very difficult.

As a result, only three of the neosuchian ecomorphotypes were analyzed. We refer to these three ecomorphotypes as “Neosuchian G” (cf. *Goniopholididae*), “Neosuchian B” (cf. *Bernissartiidae*), and “Neosuchian A” (cf. *Atoposauridae*). There are also many mammal teeth in the assemblage, including multituberculates, triconodonts, symmetrodontids, and tribosphenids. We attempted to sample mammal teeth, but we failed to recover viable sample sizes from these very small fossils with such thin enamel. Fish, lizards, and amphibians are also represented. No enamel-bearing fossils of lizards or amphibians were present in the assemblage, and these groups were not sampled. Most of these clades are represented by tens, hundreds, or thousands of specimens in the V1075 assemblage.

Powdered samples were drilled from the specimens using a Brassler NSK UM50TM dental drill with a tungsten-carbide burr. To minimize destruction of fossil resources, only a small number of specimens were selected for duplicate sampling and analysis. In some specimens, we took bulk samples across the long axis of the tooth to homogenize sampling along ontogenetic growth. Others were sampled serially to assess variation along growth axes. The densest material was targeted in each turtle skeletal fragment. For teeth, care was taken to limit sampling to enamel only, with efforts to minimize inclusion of dentine. Like bone, dentine is known to be more susceptible than enamel to diagenetic alteration of isotopic compositions due to the smaller hydroxyapatite crystals and porous texture of bone and dentine. Ganoine scales were crushed whole by mortar and pestle. For conical fish teeth (cf. *Lepistosteidae*), dentine was milled out from within the tooth, and the remaining enamel was crushed by mortar and pestle. Specimens that were too small to hold by hand while drilling were held in place on glass slides using cyanoacrylate glue. After sampling, the fossils were removed from the slides by submersion in acetone ( $C_3H_6O$ ) for 24 h. For taxa with enough specimens, at least ten specimens were sampled at least once for each taxonomic group. Drilled hydroxyapatite powders were converted to silver phosphate ( $Ag_3PO_4$ ) following (Vennemann et al., 2002; Suarez et al., 2012). Details of the silver phosphate method used in this study can be found in [Supplementary Material](#). Briefly, samples were treated with acetone to remove cyanoacrylate and then with bleach ( $NaOCl$ ) to remove organics. Powders are then dissolved in nitric acid ( $HNO_3$ ). Phosphate ions are then separated from Ca and OH ions by reacting the sample solution with KOH and KF. A silver amine solution ( $AgNO_3$ ,  $NH_4NO_3$ , and  $NH_4OH$ ) is added, resulting in the bonding of silver and phosphate ions, which are precipitated as  $Ag_3PO_4$  crystals. The  $Ag_3PO_4$  crystals are rinsed thoroughly with deionized water and dried. Yields ranged from 116 to 793  $\mu g$ . For each sample, 400–600  $\mu g$  of crystals were weighed and wrapped in silver capsules. The wrapped samples were combusted at high temperatures to produce CO gas on a Thermo TC/EA connected to a MAT 253 isotope ratio mass spectrometer (IRMS).  $\delta^{18}O$  values were corrected relative to VSMOW using NIST 80 and 81. Reproducibility was monitored by replicate analyses of Acros  $Ag_3PO_4$  ( $\sigma \sim 0.35\text{‰}$  VSMOW).

## 2.2 Paleoenvironmental reconstructions

$\delta^{18}O_{\text{phosphate}}$  (abbreviated as  $\delta^{18}O_p$ ) data from multiple taxa were used to estimate the  $\delta^{18}O$  of parent waters and the temperature

of surface waters. Reconstructing these two parameters from  $\delta^{18}O_p$  alone requires analysis of two types of taxa: taxa with constrained body temperatures (T-constrained) and taxa with body temperatures that track environmental temperature (T-unconstrained). Broadly, this multi-taxon approach involves a two-step process that leverages empirically observed relationships between  $\delta^{18}O_p$  of bioapatite,  $\delta^{18}O$  of parent water, and mineral growth temperature. First,  $\delta^{18}O_{\text{surface\_water}}$  (abbreviated as  $\delta^{18}O_{sw}$ ) is estimated from the  $\delta^{18}O_p$  of T-constrained taxa. Second,  $\delta^{18}O_{sw}$  is combined with  $\delta^{18}O_p$  of T-unconstrained taxa to solve for temperature. Here, we outline our approach to this using  $\delta^{18}O_p$  of turtles, crocodylomorphs, and fish following [Barrick et al. \(1999\)](#), [Amiot et al. \(2007\)](#), and [Fricke and Wing \(2004\)](#). R Markdown documentation of the R code used in this analysis is provided in the [Supplementary Material](#). A simple deterministic example of the multi-taxon procedure we followed is outlined below using the equations provided:

1. Applying [Equation 1](#) to the mean  $\delta^{18}O_p$  value of V1075 *Glyptops* fossils (13.8‰ VSMOW) yields a  $\delta^{18}O_{sw}$  value of  $-8.4\text{‰}$  (VSMOW).
2. Applying [Equation 2](#) to the mean  $\delta^{18}O_p$  of V1075 “Neosuchian G” fossils (14.1‰ VSMOW) yields a  $\delta^{18}O_{sw}$  value of  $-7.6\text{‰}$  (VSMOW).
3. Taking the mean  $\delta^{18}O_p$  of V1075 gar fossils (13.8‰ VSMOW), our mean measured value of the NBS120c standard (22.6‰ VSMOW), and the mean  $\delta^{18}O_{sw}$  estimate of  $-8.3\text{‰}$  (VSMOW), [Equation 3](#) provides a temperature estimate of 25°C.

$$\delta^{18}O_{sw} \text{ VSMOW} = 1.03(\pm 0.03) * (\delta^{18}O_p \text{ VSMOW}) - 22.58(\pm 0.59) \quad (1)$$

$$\delta^{18}O_{sw} \text{ VSMOW} = 0.82(\pm 0.06) * (\delta^{18}O_p \text{ VSMOW}) - 19.13(\pm 1.08) \quad (2)$$

$$T(^{\circ}C) = 117.4(\pm 5.04) - 4.19(\pm 0.21) * ((\delta^{18}O_p \text{ VSMOW} + (22.6 - \delta^{18}O_{NBS120c} \text{ VSMOW})) - \delta^{18}O_{sw} \text{ VSMOW}) \quad (3)$$

$\delta^{18}O_{sw}$  was estimated from the  $\delta^{18}O_p$  of two semi-aquatic taxa: the turtle *Glyptops* and the crocodylomorph morphotype “Neosuchian G.” Previous work has demonstrated linear relationships between  $\delta^{18}O_p$  and  $\delta^{18}O_{sw}$  for semi-aquatic turtles and crocodylians in modern settings ([Barrick et al., 1999](#); [Amiot et al., 2007](#)). Modern crocodylians and turtles thermoregulate through behavior such as sun basking, maintaining constrained body temperatures when conditions allow. Paired measurements of turtle  $\delta^{18}O_p$  and habitat  $\delta^{18}O_{sw}$  suggest that in some turtle taxa, bone growth occurs within a body temperature range of  $\sim 31^{\circ}C$ – $33^{\circ}C$  ([Barrick et al., 1999](#)). We reanalyzed [Barrick et al. \(1999\)](#) data and accurately reproduced the linear regression between  $\delta^{18}O_p$  and  $\delta^{18}O_{sw}$  (adjusted  $R^2 = 0.98$ ). The regression model we reproduced is shown as [Equation 1](#). [Amiot et al. \(2007\)](#) found a similar pattern in modern crocodylians. We reanalyzed the data from [Amiot et al. \(2007\)](#) and accurately reproduced the relationship between  $\delta^{18}O_p$  and  $\delta^{18}O_{sw}$  (adjusted  $R^2 = 0.84$ ). The regression model we reproduced from data in [Amiot et al. \(2007\)](#) is presented as [Equation 2](#).

This approach to reconstructing  $\delta^{18}\text{O}_{\text{sw}}$  relies on several assumptions. One assumption is that body water  $\delta^{18}\text{O}$  of *Glyptops* and “Neosuchian G” was not significantly influenced by factors such as seasonal variability, evaporation, or heterogeneous water sources, but rather was largely determined by habitat preference and diet (Barrick et al., 1999). Semi-aquatic ectotherms that consume mostly aquatic food sources should have body water  $\delta^{18}\text{O}$  which correlates with  $\delta^{18}\text{O}_{\text{sw}}$ . Anatomical evidence strongly suggests a semi-aquatic habit for both *Glyptops* and “Neosuchian G.” Gracile limbs and jaw elements suggest an aquatic habit and diet for pleurosternid turtles, including *Glyptops* (Evers, 2023). Cretaceous crocodylomorphs occupied a variety of habitats, including fully aquatic, semi-aquatic, and fully terrestrial (Wilberg et al., 2019). This functional diversity is represented in the V1075 crocodylomorph fauna, as suggested by the disparity in  $\delta^{18}\text{O}_{\text{p}}$  distributions between morphotypes (referred to hereafter as taxa for simplicity). However, we interpret an aquatic or semi-aquatic habit and diet for “Neosuchian G” based on: a) comparison of  $\delta^{18}\text{O}_{\text{p}}$  with sympatric taxa, and b) the presence of apicobasal ridges on the teeth. We excluded *Naomichelys*, the other easily identifiable turtle genus in the V1075 assemblage, from  $\delta^{18}\text{O}_{\text{sw}}$  reconstructions because its anatomical features indicate a terrestrial lifestyle (Joyce et al., 2015; Joyce, 2017). We excluded “Neosuchian A” and “Neosuchian B” because their reconstructed  $\delta^{18}\text{O}_{\text{water}}$  values differed significantly from “Neosuchian G” and *Glyptops*. Also, “Neosuchian A” teeth share affinities with Atoposauridae, a complex group which includes both fully terrestrial and semi-aquatic forms (Tennant et al., 2016). Another key assumption we make is that *Glyptops* and “Neosuchian G” maintained a similar range of body temperatures to that of the modern taxa that the regressions are based on. Barrick et al. (1999) found that some turtle taxa seem to demonstrate a better correlation between  $\delta^{18}\text{O}_{\text{p}}$  and  $\delta^{18}\text{O}_{\text{sw}}$  than other taxa. However, taxa with  $\delta^{18}\text{O}_{\text{p}}$  that correlated poorly with  $\delta^{18}\text{O}_{\text{sw}}$  were not sampled from a broad range of latitudes (and therefore temperature regimes), and future expansion on Barrick’s observations may show that the strong correlation between  $\delta^{18}\text{O}_{\text{p}}$  and  $\delta^{18}\text{O}_{\text{sw}}$  is true for most or all semi-aquatic turtles. Amiot et al. (2007) found that the regression between  $\delta^{18}\text{O}_{\text{p}}$  and  $\delta^{18}\text{O}_{\text{sw}}$  did not vary significantly between crocodylian taxa. The distributions of empirical  $\delta^{18}\text{O}_{\text{sw}}$  estimates from *Glyptops* and “Neosuchian G” do not differ significantly from one another, suggesting that our assumptions underlying reconstructions from *Glyptops* and “Neosuchian G” might be valid.

$\delta^{18}\text{O}_{\text{sw}}$  estimated from  $\delta^{18}\text{O}_{\text{p}}$  of T-constrained taxa (in this case *Glyptops* and “Neosuchian G”), along with  $\delta^{18}\text{O}_{\text{p}}$  of T-unconstrained taxa, can be used to estimate temperature. A strong relationship between  $\delta^{18}\text{O}_{\text{p}}$ - $\delta^{18}\text{O}_{\text{water}}$  and temperature has been demonstrated repeatedly in aquatic taxa (Longinelli, 1966; Longinelli and Nutti, 1973a; Longinelli and Nutti, 1973b; Kolodny et al., 1983). Puceat et al. (2010) presented an improved calibration using the measured value of NBS120c to correct for inter-laboratory variability. This calibration by Puceat et al. (2010) is shown as Equation 3. Garfish (Lepisosteidae, referred to here simply as “gar”) are good candidates for a T-unconstrained taxon, as they are ectotherms with limited ability to regulate their body temperature through behavior (Fricke and Wing, 2004). We used  $\delta^{18}\text{O}_{\text{p}}$  of gar teeth and scales, along with our  $\delta^{18}\text{O}_{\text{sw}}$  estimate from *Glyptops* and “Neosuchian G”, to estimate temperature using Equation 3.

Several assumptions underlie the multi-taxon approach to estimating temperature. First, we must assume that the taxa used in the reconstructions all sampled environmental waters with similar  $\delta^{18}\text{O}$ . If taxa derived their  $\delta^{18}\text{O}$  values from isotopically distinct water sources, this could lead to inaccurate temperature estimates. It is difficult to determine with high certainty whether fossil animals sampled from isotopically distinct waters, but constraints can be estimated in the case of the V1075 aquatic fauna. Interpreting the depositional environment allows constraints on inhabited water conditions. The V1075 assemblage was collected from gray mudstone facies near the base of Ostrom’s “Unit VII” in the Himes Member. Studies of the Cloverly across the Bighorn Basin suggest that gray mudstones in this interval represent deposition on a poorly drained fluvial floodplain (D’Emic et al., 2019; Orchard, 2024). Vertebrate microfossil bonebeds containing aquatic, semi-aquatic, and fully terrestrial animals within floodplain deposits are typically interpreted as *in situ* accumulations in floodplain wetlands (Rogers et al., 2007; Rogers and Brady, 2010). The V1075 fossils likely accumulated in such an environment, as there is no evidence in the Cloverly of large, deep lakes, and the V1075 assemblage is hosted in fine-grained deposits inconsistent with channel-lag deposits. Still, we can’t know if these floodplain wetlands were ever connected at the surface with nearby stream channels, or if the V1075 aquatic taxa moved between these wetlands and stream channels. Time spent in a river channel which drained higher elevation uplands could have exposed some of the V1075 aquatic fauna to lower  $\delta^{18}\text{O}$  than that of the local floodplain wetlands.

To derive an accurate and useful multi-taxon temperature estimate, we must also make assumptions about the seasonality of skeletal growth in the taxa used. The multi-taxon approach relies on the assumption that the two taxa grew their skeletal material during approximately the same seasonal period. This assumption is critical because  $\delta^{18}\text{O}$  values of precipitation can vary significantly between seasons. If the two taxa incorporated oxygen from meteoric waters into their skeletal phosphates at different times of the year, their body waters would likely reflect distinct  $\delta^{18}\text{O}$  values during skeletal growth, resulting in inaccurate temperature estimates. Also, for meaningful comparison with other temperature data, it is necessary to estimate which part of the annual temperature cycle the multi-taxon estimate represents.

Our multi-taxon  $\delta^{18}\text{O}$ -derived temperature estimate likely reflects the mean warm-season temperature of the local floodplain wetlands. However, it is challenging to determine which portion of the annual climate cycle the Cloverly ectothermic taxa recorded during tissue growth. In general, ectothermic metabolic activity peaks when habitat temperatures reach the upper range of a species’ thermal niche (Neubauer and Andersen, 2019). This is demonstrated for turtles and crocodylians by Barrick et al. (1999) and Amiot et al. (2007). Yet, it remains unclear during which months of the year the Cloverly semi-aquatic turtles and crocodylomorphs could sustain such warm, stable body temperatures. This uncertainty also applies to V1075 gar, as the growth regime of modern gar is not well understood. However, general metabolic temperature requirements in ectotherms suggest it likely that Cretaceous gar species also favored warm-season temperatures. While “warm season” cannot be precisely defined in this context, we interpret the multi-taxon temperature estimate as representative of the mean temperature during the warmest half of the year.

To account for all sources of uncertainty, we employed a Monte Carlo approach to estimate the uncertainty surrounding our mean proxy estimates by simulating many potential outcomes based on the variability in our  $\delta^{18}\text{O}_p$  data and the associated regression model parameters. Specifically, for each proxy measurement, we generated thousands of synthetic datasets by randomly sampling from normal distributions defined by the means and standard deviations of the observed values. Additionally, we incorporated the uncertainty in the regression model coefficients (intercept and slope) by sampling these parameters from their respective distributions, defined by their standard errors. Residual variability, representing unexplained error in the model, was also simulated and added to each estimate. This approach allowed us to propagate all sources of uncertainty (measurement error, regression uncertainty, and residual variability) into the final estimates. By aggregating the results of these simulations, we calculated a mean estimate and 95% confidence intervals, providing a robust quantification of uncertainty around our mean estimates.

## 3 Results

### 3.1 Oxygen isotope analyses

We generated a large multi-taxon  $\delta^{18}\text{O}_p$  dataset and used it to characterize variation across taxa and ecomorphotypes. Single measurements ranged from 9.5‰ to 23.2‰ (VSMOW), with ecomorphotype means spanning 12.0‰–19.1‰. Some taxa showed substantial within-specimen or within-taxon variation. Notably, neosuchian crocodyliforms displayed significant differences among ecomorphotypes, and terrestrial taxa such as sauropods and ornithischians yielded consistently higher  $\delta^{18}\text{O}_p$  values. These data establish the isotopic framework for interpreting water source and paleoenvironmental differences among taxa.

$\delta^{18}\text{O}_p$  results are shown in Table 1 and Figure 3A, and are available in Supplementary Material. Single measurements averaged 15.2‰ (VSMOW) and ranged from a minimum of 9.5‰ (villiform fish tooth, cf. Lepisosteidae) to a maximum of 23.2‰ (small theropod tooth, cf. *Deinonychus sp.*). To minimize destruction of specimens, most specimens were sampled only enough for one analysis (>600  $\mu\text{g}$ ). However, we sampled some specimens for duplicate analyses. Variability within individual specimens ranged from  $\sigma = <0.1\%$  to  $\sigma = 1.9\%$  (VSMOW). Only two specimens, a gar and an aquatic turtle, showed individual variation greater than  $\sigma = 1$ . Mean  $\delta^{18}\text{O}_p$  values by ecomorphotype range from a minimum of 12.0‰ relative to VSMOW (hybodontiform sharks) to a maximum of 19.1‰ (Sauropoda). Measurements from tooth enamel of the semi-aquatic “Neosuchian G” ecomorphotype (cf. Goniopholididae,  $\sigma = 2.9\%$  VSMOW) averaged 14.2‰, ranging from a minimum individual measurement of 9.8‰ to a maximum of 17.6‰. In addition to enamel, we also analyzed dentine from two “Neosuchian G” teeth. These resulted in values of 16.8‰ and 15.9‰. On average, we found that molariform crocodylian teeth (cf. Bernissartiidae, “Neosuchian B”) and spatulate crocodylian teeth (cf. Atoposauridae, “Neosuchian A”) yielded significantly more positive  $\delta^{18}\text{O}_p$  values than “Neosuchian G”. “Neosuchian B”  $\delta^{18}\text{O}_p$  values ranged from 13.1‰ to 19.2‰, with an average of 16.6‰ ( $\sigma = 1.9\%$ ). “Neosuchian A” averaged 17.0‰ ( $\sigma = 2.2\%$ ), ranging from a minimum of 15.1‰ to a maximum of 23.1‰.

Ornithischian teeth composition ranged from 13.5‰ to 19.5‰, with an average of 15.5‰ ( $\sigma = 2.1\%$ ). Sauropod tooth enamel averaged 17.6‰ ( $\sigma = 1.9\%$ ) with individual measurements ranging from 15.1‰ to 22.5‰. Lepisosteid scale (mean = 14.5‰,  $\sigma = 1.5\%$ ) and teeth (mean = 12.9,  $\sigma = 2.0\%$ ) values range from a minimum individual measurement of 9.5‰ to a maximum of 16.2‰. Carapace fragments of the semi-aquatic turtle *Glyptops sp.* (mean = 14.1‰,  $\sigma = 1.8\%$ ) ranged in  $\delta^{18}\text{O}_p$  from a minimum individual measurement of 11.1‰ to a maximum of 17.1‰. The terrestrial turtle *Naomichelys sp.* ( $\sigma = 0.6\%$ ) showed an average  $\delta^{18}\text{O}_p$  of 14.3‰, with values ranging from 13.3‰ to 15‰. Small theropod specimens (maniraptoran teeth) showed  $\delta^{18}\text{O}_p$  values ranging from a minimum of 12.7‰ to a maximum of 23.2‰, with a mean of 15.8‰. One large theropod (allosauroid) tooth was available for sampling, which yielded a mean  $\delta^{18}\text{O}_p$  of 14.7‰ from four serial samples taken along the growth axis ( $n = 3$ ,  $\sigma = 0.16\%$ ).

### 3.2 Surface water $\delta^{18}\text{O}$ and temperature reconstructions

Using  $\delta^{18}\text{O}_p$  values from turtles, crocodylomorphs, gar, and a co-analyzed standard (NBS120c), we conducted Monte Carlo simulations and deterministic calculations to estimate surface water  $\delta^{18}\text{O}$  ( $\delta^{18}\text{O}_{sw}$ ) and reconstruct paleotemperature. Simulated  $\delta^{18}\text{O}_{sw}$  values ranged from  $-11.2\%$  to  $-3.6\%$  (95% CI), and deterministic estimates were in close agreement. Combining distributions yielded a mean  $\delta^{18}\text{O}_{sw}$  of  $-7.9\%$  (95% CI:  $-10.1$ ,  $-5.5\%$ ). Applying temperature equations to these values, we estimate a mean surface water temperature of 26°C (95% CI: 8, 43°C). This is the first quantitative paleotemperature reconstruction of the Cloverly environment.

We also simulated probability distributions of coefficients and errors for the Barrick et al. (1999), Amiot et al. (2007), and Puceat et al. (2010) regressions. We simulated  $\delta^{18}\text{O}_p$  distributions for each turtle and crocodylomorph taxon, as well as for gar and NBS120c based on our measured values for each. The mean  $\delta^{18}\text{O}_p$  (VSMOW) estimates, along with their 95% confidence intervals, were as follows: 13.8‰ (12.7, 14.9‰) for *Glyptops*, 14.0‰ (12.5, 15.6‰) for “Neosuchian G,” 13.8‰ (13.0, 14.5‰) for gar, and 22.6‰ (22.4, 22.7‰) for NBS120c. We then simulated  $\delta^{18}\text{O}_{sw}$  reconstructions for each of the turtle and crocodylomorph groups. The estimated mean  $\delta^{18}\text{O}_{sw}$  values and their 95% confidence intervals are shown in Figure 3B. The mean simulated  $\delta^{18}\text{O}_{sw}$  (VSMOW) estimate for *Glyptops* is  $-8.3\%$  (95% CI:  $-10.5$ ,  $-6.0\%$ ). For “Neosuchian G,” the mean estimate is  $-7.5\%$  (95% CI:  $-11.2$ ,  $-3.6\%$ ). For comparison with our simulated values, we made simple deterministic calculations of  $\delta^{18}\text{O}_{sw}$  for each empirical  $\delta^{18}\text{O}_p$  value for *Glyptops* using Equation 1 and for “Neosuchian G” using Equation 2. The mean calculated  $\delta^{18}\text{O}_{sw}$  value for *Glyptops* was  $-8.3\%$  ( $\sigma = 0.6\%$ ). For “Neosuchian G,” it was  $-7.6\%$  ( $\sigma = 0.7\%$ ). The deterministic  $\delta^{18}\text{O}_{sw}$  distributions for *Glyptops* and “Neosuchian G” are not significantly different ( $p = 0.43$ ). We combined the two simulated  $\delta^{18}\text{O}_{sw}$  distributions and ran a Monte Carlo simulation on them to produce a single probabilistic distribution of  $\delta^{18}\text{O}_{sw}$ . The mean of simulated  $\delta^{18}\text{O}_{sw}$  means is  $-7.9\%$  (95% CI:  $-10.1$ ,  $-5.5\%$ ). To calculate a mean temperature value and construct a 95% confidence interval, we applied Equation 3 using the simulated distributions of the

**TABLE 1** Oxygen isotope analysis of OMNH-V1075 vertebrate phosphates relative to V-SMOW. *Glyptops* and *Naomichelys* values are from cortical carapace bone. Lepisosteidae values are from ganoine scales. All other measurements are from tooth enamel.

Taxon	$\delta^{18}\text{O}_p$	$N_{\text{samples}}$	Min, ‰	Max, ‰	$\sigma$	SE
<i>Glyptops</i> sp.	14.1	8	11.1	17.1	1.8	0.6
“Neosuchian A”	17.0	12	15.1	23.1	2.2	0.6
“Neosuchian B”	16.6	11	13.1	19.2	1.9	0.6
“Neosuchian G”	14.2	14	9.8	17.6	2.8	0.7
Lepisosteidae	14.0	22	9.5	16.2	1.8	0.4
Allosauroidea	14.7	4	14.3	15.1	0.3	0.2
Ornithischia	15.5	8	13.5	19.5	2.1	0.7
Sauropoda	18.1	10	15.1	22.5	2.4	0.8
Hybodontiformes	11.9	3	9.8	15.3	2.9	1.7
Maniraptorans	15.8	10	12.7	23.2	3.2	1.0
<i>Naomichelys</i> sp.	14.3	10	13.3	15.0	0.6	0.2

three variables:  $\delta^{18}\text{O}_{\text{sw}}$ ,  $\text{gar } \delta^{18}\text{O}_p$ , and NBS120c  $\delta^{18}\text{O}_p$ . The mean temperature estimate is 26°C (95% CI: 8, 43°C).

### 3.3 Water-air temperature conversion

To contextualize the temperature reconstruction, we converted the estimated mean annual warm season water temperature (26°C) into a mean annual warm season air temperature (24°C; 95% CI: 8, 41°C) using a regression model from modern lake and climate data. While prior work cautions against applying such transforms in warm climates, reanalysis of modern datasets supports a moderate correlation between warm season water temperatures and air temperatures in climates with MAAT >12°C. We also estimated a mean annual water temperature of ~19°C based on an assumed seasonal range in temperatures.

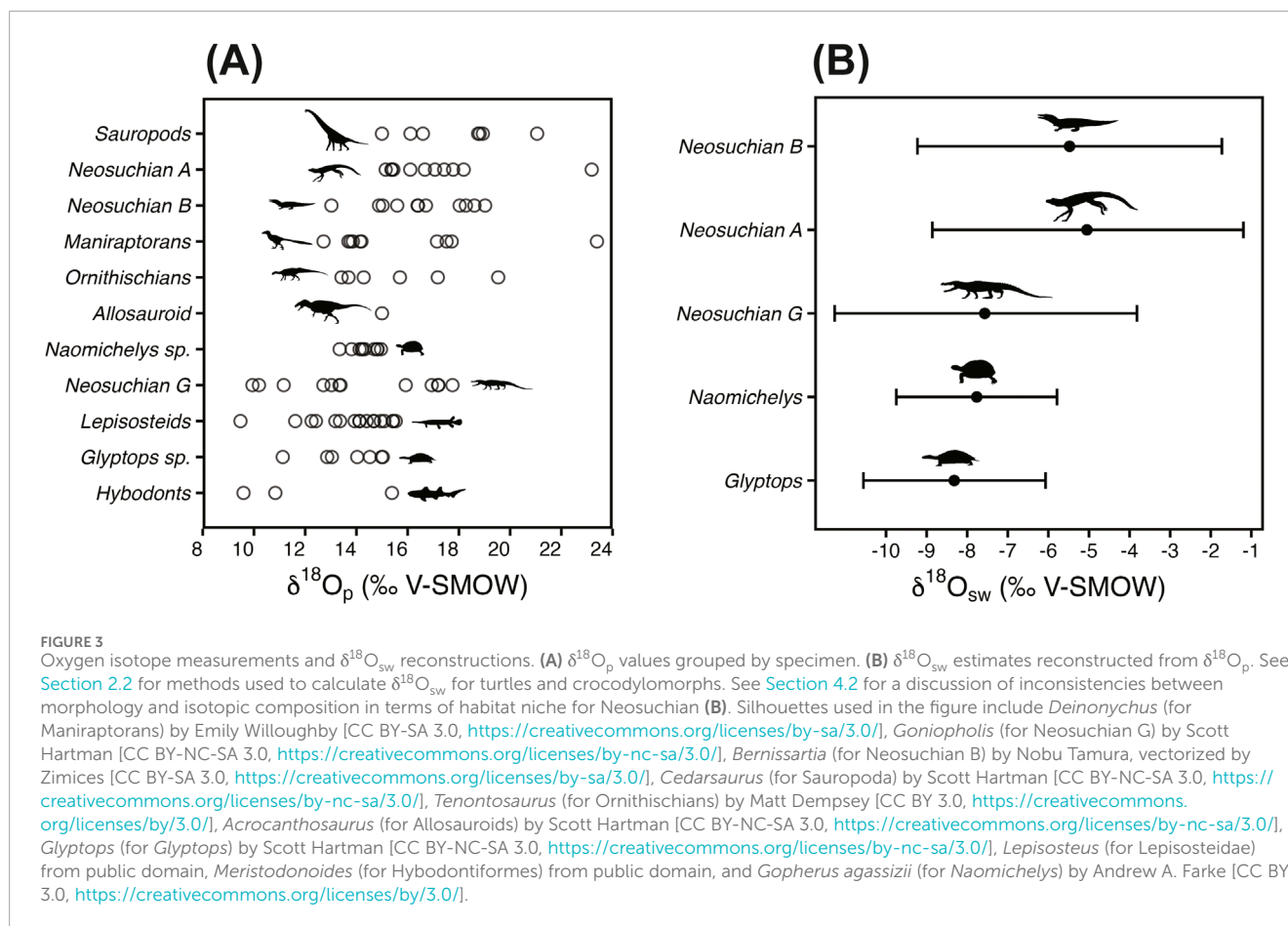
The conversion of our mean annual warm season water temperature (26°C) to mean annual warm season air temperature (24°C) utilized data from modern lakes. Modern lake and air temperature data from Hren and Sheldon (2012) indicated that while MAWSAT and MAAT are closely related in many settings, there is no significant relationship in climates with mean annual air temperature (MAAT) above 12°C–15°C. It is likely that Albian MAAT in the Cloverly region was greater than 15°C, and so this setting is not appropriate for any of the water-air temperature transform functions defined by Hren and Sheldon (2012). However, we reanalyzed data from Hren and Sheldon (2012) and found that even in climates with MAAT above 12°C, there is a significant relationship ( $p = 9 \times 10^{-12}$ ), albeit moderately strong (adjusted  $R^2 = 0.55$ ), between the mean water temperature and mean air temperature during the warm season (i.e., April–September). Given our MAWSWT estimate of 26°C, and assuming a mean annual range of temperatures (MART) of ~20°C–25°C based on

previous estimates for this region during the Campanian, we estimate a minimum mean annual water temperature (MAWT) of ~19°C. This simple estimate assumes that MAWT = MAWSWT – (MART/4). Assuming a similar MART to the Campanian of this region is justified because the paleolatitude and global temperature regime in the Albian were comparable to those of the Campanian (Burgener et al., 2019). With an estimated MAWT well above 12°C, we find it justified to apply our MAWSWT-MAWSAT regression model to our V1075 MAWSWT estimate. In doing so, we find that the model predicts a MAWSAT of 24°C (95% CI: 8, 41°C).

### 3.4 Error analysis

Our temperature estimates varied considerably, and our mean estimate is highly uncertain. We performed a series of targeted Monte Carlo simulations to estimate the relative contributions of error from each input and regression coefficient. We conducted a series of Monte Carlo simulations to assess different sources of uncertainty to the total variance in the estimates of  $\delta^{18}\text{O}_{\text{sw}}$  and temperature. Using 1,000 iterations, we varied synthetic  $\delta^{18}\text{O}_p$ , regression slope, intercept, and residual error simultaneously to calculate the total variance of the model outputs. We then performed targeted simulations, varying one input at a time while keeping the others fixed at their mean values, to isolate the variance contributed by each input. The variance contributions were normalized by the total variance to determine their relative importance. The variance contributions to the total uncertainty in  $\delta^{18}\text{O}_{\text{sw}}$  and temperature estimates are distributed across several sources.

For  $\delta^{18}\text{O}_{\text{sw}}$  reconstructions from both *Glyptops* and “Neosuchian G,” residual error in the underlying regression models from Barrick et al. (1999) and Amiot et al. (2007) was the largest source of uncertainty, contributing approximately 31% and 35%



of the total variance, respectively. The regression intercept also contributed significantly, accounting for 26% of the variance for *Glyptops* and 32% for Neosuchian G, reflecting uncertainty in the baseline offset between  $\delta^{18}O_p$  and  $\delta^{18}O_{sw}$ . Slope error accounted for 17% of the variance for *Glyptops* and 21% for Neosuchian G. Variability in  $\delta^{18}O_p$  contributed 25% for *Glyptops* but only 12% for “Neosuchian G”. While  $\delta^{18}O_p$  variability was a notable factor, the dominant sources of uncertainty were the residual error and intercept variability, underscoring the limitations of the regression models in precisely capturing the relationship between  $\delta^{18}O_p$  and  $\delta^{18}O_{sw}$ . These results highlight the importance of addressing residual noise and refining regression parameters to improve the precision of this approach to  $\delta^{18}O_{sw}$  reconstructions in the future.

For temperature reconstructions, we were unable to reproduce the pooled regression presented by Puceat et al. (2010). The Puceat et al. (2010) pooled regression combined new data with previously published data from Longinelli and Nuti (1973a) and Kolodny et al. (1983). We compiled the Puceat et al. (2010) data and the Longinelli and Nuti (1973b). We were unable to reproduce the Kolodny et al. (1983) data as presented in Puceat et al. (2010). We performed a regression analysis on the combined Puceat et al. (2010) and Longinelli and Nuti (1973a) data and found that the regression coefficients and errors were very similar to those reported by Puceat et al. (2010) for their pooled model, suggesting that the model we present here is comparable in accuracy and precision. We used Monte Carlo simulations to evaluate the relative error contributions

of slope, intercept, residual error,  $\delta^{18}O_{sw}$ , and  $\delta^{18}O_p$ . The results indicate that  $\delta^{18}O_{sw}$  contributes the most uncertainty (~40% of the total variance) to the temperature estimates. Intercept (29%) and slope (28%) were also significant contributors of error.  $\delta^{18}O_p$  (1%) and NBS120c (<1%) contributed comparatively negligible errors. This demonstrates the high sensitivity of the temperature regression to variability of  $\delta^{18}O_{sw}$  inputs, as well as the need for additional data to more precisely calibrate the regression model.

Error analysis of the MAWSAT estimate indicates that uncertainty in the MAWSAT estimate is the dominant source of error, significantly outweighing the contributions from the regression coefficients and residual error in the transformation function. While the transform function is only based on a moderately strong relationship (adjusted  $R^2 = 0.55$ ), the propagated error from  $\delta^{18}O_{sw}$  through the temperature calculations is the largest contributor to the total uncertainty, far exceeding the error introduced by the regression model itself.

## 4 Discussion

### 4.1 Isotopic evidence of ecological niche partitioning

Inter-taxon comparisons of  $\delta^{18}O$  reveal evidence for resource partitioning among the Cloverly fauna. Significant offsets between

reconstructed  $\delta^{18}\text{O}_{\text{sw}}$  values of some crocodylomorph taxa suggest distinct habitat preferences. Although we did not reconstruct  $\delta^{18}\text{O}_{\text{sw}}$  from dinosaur or fish  $\delta^{18}\text{O}_{\text{p}}$ , we can make qualitative inferences based on the offsets between groups. For most V1075 taxa, the observed isotopic niches generally correspond with the paleobiological frameworks inferred previously from other evidence. However, there are exceptions, as discussed below.

Both turtle and crocodylomorph lineages have repeatedly adapted to terrestrial and aquatic habitats throughout their evolutionary histories. Comprehensive anatomical descriptions or a clear phylogenetic framework is required to infer an aquatic or terrestrial habit for a fossil taxon in either of these groups. Many turtle and crocodylomorph fossil occurrences in Cretaceous deposits are based on isolated elements or incomplete skeletons. Thus, contextual information is often missing that would help distinguish aquatic and terrestrial taxa. Atoposaurid-like teeth (“Neosuchian A”) from V1075 also result in  $\delta^{18}\text{O}_{\text{sw}}$  reconstructions consistent with the terrestrial habitat inferred from morphology of body fossils of similar taxa in other Mesozoic assemblages. Atoposaurid-like teeth from mid-Cretaceous deposits have occasionally been referred to the terrestrial genus *Theriosuchus* sp. (e.g., Winkler et al., 1990; Cifelli et al., 1999). Although no *Theriosuchus* or other atoposaurid body fossils are known from Aptian-Albian deposits in North America, a small terrestrial paralligatorid (*Wanchaampsus kirpachi*) has been described from the Aptian of Texas (Adams, 2015). The atoposaurid-like teeth from the V1075 assemblage may have belonged to a similar terrestrial paralligatorid in the Cloverly region during the Albian. Paralligatorids and atoposaurids are thought to have diverged from a common ancestor sometime in the Jurassic, and recent phylogenetic analyses suggest that Atoposaurids were likely extinct by the Early Cretaceous (Tennant et al., 2016). North American Cretaceous teeth like those that we refer to here as the “Neosuchian G” morphotype have traditionally been treated as belonging to Goniopholididae. Although the true phylogeny of the Cloverly goniopholid-like tooth-bearer is unclear, the “Neosuchian G” teeth show marginal carina and apicobasal ridges that suggest aquatic feeding adaptations like that of goniopholids (McCurry et al., 2019). Our data show agreement between functional morphology and isotopic niche in the V1075 “Neosuchian A” and “Neosuchian G” forms. The turtles *Naomichelys* and *Glyptops* show very similar  $\delta^{18}\text{O}_{\text{p}}$  distributions, averaging higher than most aquatic taxa and lower than most terrestrial taxa. This pattern is consistent with a semi-aquatic habitat preference and suggests that their isotopic niche accurately reflects their habitat niche.

Unlike the other V1075 taxa,  $\delta^{18}\text{O}_{\text{p}}$  of molariform crocodylomorph teeth (cf. Bernissartiidae, referred herein as “Neosuchian B”) are not consistent with morphological and isotopic interpretations of habitat in Bernissartiid-like crocs from other Mesozoic assemblages. Based on a brevirostrine skull shape and durophagous tooth morphology, earliest Cretaceous bernissartiids from Europe were assumed to having been semi-aquatic, feeding largely on freshwater molluscs whose fossils are numerous in the Wealden of the Isle of Wight (Buffetaut and Ford, 1979; Sweetman et al., 2014; Martin et al., 2020). This was supported by the interpretation of the sediment facies of the Lower Cretaceous Wealden deposits as representing a seasonal wetland to lacustrine

paleoenvironment (Spagna et al., 2012). Likewise, Bernissartiid-like teeth from the Cenomanian of Utah have been interpreted as having been from a semi-aquatic animal based on relatively low oxygen isotopes from tooth phosphate (Suarez et al., 2014; Pouech et al., 2014). In contrast,  $\delta^{18}\text{O}_{\text{p}}$  values from V1075 “Neosuchian B” are higher than those of most aquatic and semi-aquatic forms in the assemblage. There are several scenarios that are most likely to have resulted in relative isotopic enrichment in the V1075 “Neosuchian B” teeth. One possibility is that there is more functional and taxonomic diversity represented by isolated mid-Cretaceous molariform crocodylomorph teeth than what has previously been thought. As with the Cloverly “Neosuchian G” teeth, the phylogenetic placement of “Neosuchian B” is somewhat uncertain. Although Aptian-Albian molariform neosuchian teeth in North America have often been attributed to or compared with the Bernissartiidae from the Barremian-Hauterivian of Europe and Africa, there are no known body fossils of bernissartiids from North American deposits (Ullmann et al., 2011; Oreska et al., 2013). It is possible that the V1075 “Neosuchian B” teeth belonged to a paralligatorid crocodylomorph that adapted to terrestrial environments. Although evolutionary habitat shifts between the terrestrial, freshwater, and marine realms are common in the crocodylomorph fossil record, these shifts usually correspond with major phylogenetic divergence rather than at the species or genus level (Wilberg et al., 2019). Bernissartia diverged from Paralligatoridae in the middle Jurassic, and Crocodylia evolved from paralligatorids. Some Crocodylian lineages are thought to have adapted from freshwater to terrestrial environments in the late Cenozoic, so it is plausible that a terrestrial durophagous paralligatorid may have lived in the Cloverly region during the Albian (Montefeltro et al., 2013; Joyce et al., 2015; Joyce, 2017; Wilberg et al., 2019). This scenario cannot be ignored given the coarse diagnostic utility of crocodylomorph teeth and the paucity of bernissartiid body fossils in mid-Cretaceous deposits. In addition, the Bernissartiid-like teeth analyzed by Suarez et al. (2014) are likely millions of years younger than those presented here, and this invokes possible evolutionary differences between these two forms. Another explanation might be that the Cloverly bernissartiid was in fact aquatic like its confamilial relatives, but that its  $\delta^{18}\text{O}_{\text{sw}}$  was higher due to time spent in high- $\delta^{18}\text{O}$  waters. If we assume this is the case, there are two most likely sources of high- $\delta^{18}\text{O}$  surface waters that would have been available in the Cloverly environment. Either the water body was evaporatively enriched in  $^{18}\text{O}$  relative to precipitation (lake or pond), or it was influenced by seawater (estuary). With  $\delta^{18}\text{O}$  alone, it is impossible to discern between the two. If we assume that “Neosuchian B”  $\delta^{18}\text{O}_{\text{sw}}$  was higher due to time spent in an estuarine or marine environment, we must infer that “Neosuchian B” adapted a higher salinity tolerance than other V1075 crocodylomorphs, turtles, and fish sampled in this study. Another possible explanation might be that “Neosuchian B” spent more time sun basking than other amphibious reptile taxa in the V1075 fauna. Any one of the scenarios given above might have resulted in higher body water  $\delta^{18}\text{O}$  in “Neosuchian B” relative to presumed aquatic taxa (“Neosuchian G” and *Glyptops*). Regardless of what combination of factors resulted in higher  $\delta^{18}\text{O}_{\text{sw}}$  in “Neosuchian B,” it is evident that this taxon differed from co-occurring aquatic reptiles in habitat or thermoregulatory behavior.

There are no established methods for reconstructing body water  $\delta^{18}\text{O}$  from dinosaurs, although some have attempted to use mammal-derived empirical regressions to do so (Cullen et al., 2020). This is problematic due to assumptions about analogous physiology between mammals and dinosaurs and because these equations require quantitative constraints on atmospheric humidity, which are currently unavailable for the Cloverly (Kohn, 1996). However, qualitative inferences about the  $\delta^{18}\text{O}$  composition of body water in the V1075 dinosaur fauna can be made if we assume that the  $\delta^{18}\text{O}_p$  distributions reflect patterns in body water composition. Sauropods show the highest  $\delta^{18}\text{O}_p$  values of any dinosaur group in the assemblage. This is consistent with  $\delta^{18}\text{O}_p$  datasets from many other sauropod-bearing Cretaceous assemblages and has been attributed to the higher isotopic composition of the water in their leafy diet (Amiot et al., 2011; Suarez et al., 2014; Amiot et al., 2015; Amiot et al., 2021). On average, ornithischians from the V1075 assemblage generally have lower  $\delta^{18}\text{O}_p$  values than the sauropods. This could be explained by food resource partitioning, differences in physiology, differences in habitat preference, or differences in water consumption (ratio of food water and drinking water). Maniraptoran  $\delta^{18}\text{O}_p$  values are more like ornithischians than sauropods, but all the dinosaurian groups show higher average  $\delta^{18}\text{O}_p$  values than the aquatic and semi-aquatic taxa. We analyzed two fish taxa: Lepisosteidae and Hybodontiformes. Both groups show similar  $\delta^{18}\text{O}_p$  distributions with lower means than any other V1075 taxa.

## 4.2 Implications for mid-Cretaceous paleoclimate

As seen in Figure 4, our reconstructed  $\delta^{18}\text{O}_{sw}$  values are generally consistent with proxy-based  $\delta^{18}\text{O}_{sw}$  reconstructions from other assemblages in the Western Interior when adjusted for paleolatitude (Suarez et al., 2014; Suarez et al., 2021; Harper et al., 2021). Previous reconstructions of  $\delta^{18}\text{O}_{sw}$  in the mid-Cretaceous Western Interior significantly underestimated paleolatitude. Recent tectonic modeling suggests a paleolatitude of  $\sim 52^\circ\text{N}$  at 110 Ma for the Cloverly, roughly  $10^\circ\text{N}$  higher than previously assumed for the Cloverly (Suarez et al., 2014; van Hinsbergen et al., 2015; Suarez et al., 2021; Vaes et al., 2023). Adjusted for these newer paleolatitudinal reconstructions,  $\delta^{18}\text{O}_{sw}$  reconstructions plot near the gradient of modern  $\delta^{18}\text{O}_{precipitation}$ , and well above the range modeled for the Aptian-Albian by Suarez et al. (2011). However, this modeled  $\delta^{18}\text{O}_{precipitation}$  range presented originally by Suarez et al. (2011) is almost certainly an underestimate given the following. The Suarez model reconstructed a theoretical  $\delta^{18}\text{O}_{precipitation}$  gradient by combining a large empirical dataset of  $\delta^{18}\text{O}_{carbonate}$  (sideritic and calcitic calcretes) with several latitudinal temperature gradients previously modeled for the mid Cretaceous (Barron, 1983; Ufnar et al., 2002; Zhou et al., 2008). These models were based on underestimated paleolatitude parameters. This could also cause shifts in the latitudinal reconstruction such that what was previously thought to be relatively low  $\delta^{18}\text{O}_{precipitation}$  values are more in line with expectations at more northerly latitudes. In addition, the Suarez model assumes carbonate  $\delta^{18}\text{O}$  reflects mean annual surface water values, rather than a seasonally-biased estimate. Evidence increasingly suggests that soil carbonates

typically (with some exceptions) form in the warm months and thus record seasonal bias towards summer conditions (Breecker et al., 2009; Peters et al., 2013; Burgener et al., 2016; Huth et al., 2019; Kelson et al., 2020). Seasonal biases in temperature estimates may have led Suarez et al. (2011) and Ufnar et al. (2002) to underestimate temperatures in calculation of  $\delta^{18}\text{O}_{precipitation}$ . This would have the effect of lowering the  $\delta^{18}\text{O}$  of water reconstructions. We expect that an updated model will shift the predicted  $\delta^{18}\text{O}_{precipitation}$  range closer to the modern gradient and corroborate that the Western Interior vertebrate  $\delta^{18}\text{O}_p$  water isotope reconstructions, including those from V1075, will be consistent with warm-season averages.

Many of the taxonomic groups in our dataset show considerable scatter in  $\delta^{18}\text{O}_{phosphate}$  values, which we interpret as being due in part to short-term climatic variability. Given the geologically short period of time that our data represents ( $10^4$ – $10^2$  years of time averaging), we can rule out the influence of orbitally-forced ( $10^5$  yrs) climate fluctuations (Rogers et al., 2007; Rogers and Brady, 2010). In highly mobile taxa, some of this scatter may be attributed to movement between isotopically distinct reservoirs. For example, fish may have migrated between floodplain wetlands, tributary streams that were primarily sourced by local precipitation (higher  $\delta^{18}\text{O}$ ), low-order (trunk) rivers with lower  $\delta^{18}\text{O}$  water influenced by high-elevation catchments in the Sevier highlands, and perhaps even brackish estuaries on the WIS coastal margin. Likewise, it is plausible that some Cloverly dinosaurs may have inhabited broad geographic ranges, or at least occasionally migrated to other parts of the region and ingested waters from a variety of reservoirs. Behavioral influence aside, climatic factors that may have contributed to the scatter would be different between habitat types. Some of the dinosaur taxa represented in our dataset show some degree of positive skew in their  $\delta^{18}\text{O}_p$  distributions. This positive skew may indicate periods of arid conditions with increased evaporation precipitation ratios and/or a significant decrease in relative humidity, either of which might have increased  $\delta^{18}\text{O}_{body\_water}$  in those taxa. Conversely, there are low outlier  $\delta^{18}\text{O}_p$  values in the aquatic and semi-aquatic taxa. This may indicate periods of high summer rainout effect or periods of increased runoff from the Sevier Highlands.

The MAWSAT estimate of  $24^\circ\text{C}$  (95% CI:  $10$ ,  $41^\circ\text{C}$ ) falls within a range predicted previously by proxy-model data assimilation for this paleolatitude and is on trend with other Aptian-Albian empirical estimates from the WIB (Figure 4; Judd et al., 2024). The Albian saw a transition from Early Cretaceous normal greenhouse conditions to the extreme hothouse conditions of the early Late Cretaceous. Between the beginning and end of the Albian stage, global sea surface temperatures increased by roughly  $10^\circ\text{C}$  (O'Brien et al., 2017). Our estimate of  $24^\circ\text{C}$  suggests that Albian MAAT might have been  $\sim 10^\circ\text{C}$  higher than today in the Bighorn Basin region. If accurate, this estimate implies that temperatures in the Bighorn Basin region during the mid-late Albian were still  $\sim 10^\circ\text{C}$  cooler during Cloverly deposition than during the following Cretaceous Thermal Maximum. This generally agrees with previous reconstructions of the global temperature trend from Albian to Turonian time (O'Brien et al., 2017; Grossman and Joachimski, 2022; Judd et al., 2024). Our estimated warm-season air temperature of  $24^\circ\text{C}$  includes a wide uncertainty range ( $10^\circ\text{C}$ – $41^\circ\text{C}$ ) yet falls within the range of values expected during the broader warming

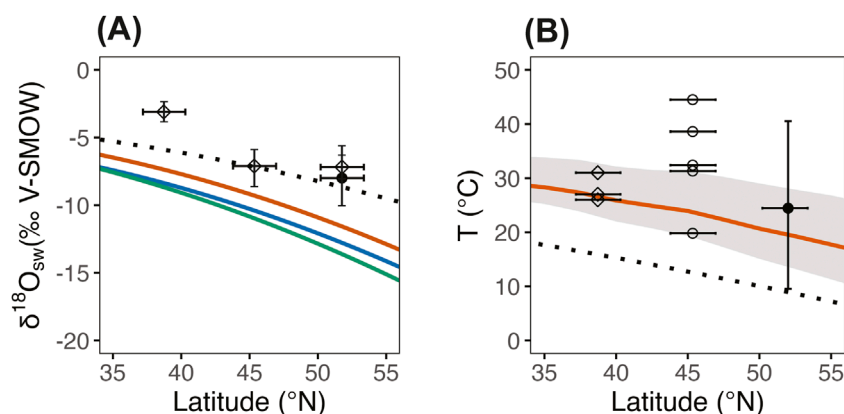


FIGURE 4

V1075 geochemical proxy reconstructions compared with modeled latitudinal gradients and existing proxy data from the Aptian–Albian nonmarine WIB. (A)  $\delta^{18}\text{O}$  of precipitation. 95% confidence intervals around mean  $\delta^{18}\text{O}_{\text{sw}}$  estimates. The closed circle represents the mean probabilistic  $\delta^{18}\text{O}_{\text{sw}}$  estimate from this study. Diamonds represent deterministic mean of  $\delta^{18}\text{O}_{\text{sw}}$  estimates from turtle  $\delta^{18}\text{O}_p$  as reported by Suarez et al., 2021; Suarez et al., 2021 sampled from a variety of turtle taxa, including specimens not identifiable to the sub-family taxonomic level. Dotted line represents the modern  $\delta^{18}\text{O}_{\text{sw}}$  gradient as presented by Rozanski et al. (1993). The colored lines represent each of the  $\delta^{18}\text{O}_{\text{sw}}$  models currently available for the mid-Cretaceous. The red line is a model by Suarez et al. (2011) based on the “Warm Cretaceous” temperature scenario modelled by Barron (1983). The blue represents the Suarez et al. (2011) model based on Barron’s (1983) “Cool Cretaceous” temperature model. The green represents a coupled ocean-atmosphere general circulation model (GENESIS-MOM) gradient predicted for the mid-Cretaceous by Zhou et al. (2008). Paleolatitudes and 95% CI estimates are based on the tectonic model by Vaes et al. (2023). Note that the proxy data from multiple Aptian–Albian sites in the WIB agree better with the modern  $\delta^{18}\text{O}_{\text{sw}}$  gradient than with predictions from models of the Cretaceous (Suarez et al., 2011; Zhou et al., 2008). See Section 4.3 for discussion on data-model mismatch. (B) Temperature by latitude. The red line and the grey ribbon represent the mean annual global sea surface temperature and 95% CI as predicted by model-proxy data assimilation by Judd et al. (2024). Closed circle represents the mean MAWSAT estimate from this study. Open diamonds are estimates from hydrogen and oxygen isotopes of paleosol phyllosilicates in the Antlers Fm. Of Oklahoma reported by Andrzejewski and Tabor, (2020). Open circles are estimates from “clumped isotopes” ( $\Delta_{47}$ ) of pedogenic carbonates in the Ruby Ranch Mbr. of the Cedar Mountain Formation in Utah (Suarez et al., 2021). Note that all temperature proxy data generally plot above mean annual global sea surface temperature. 95% CI is shown for the V1075 temperature estimate, but confidence intervals were not constructed around estimates from Andrzejewski and Tabor. (2020) and Suarez et al. (2021).

trend from the Aptian–Albian Cold Snap to the Cretaceous Thermal Maximum. We interpret our estimate as an annual mean of warm season temperatures, and if this is true, then it follows that our value would be higher than most MAAT estimates. Marine  $\text{TEX}_{86}$  and  $\delta^{18}\text{O}$  data suggest that the warming between the Aptian–Albian Cold Snap and the Cretaceous Thermal Maximum occurred in pulses during the early-mid Albian, the late Albian, and then again in the late Cenomanian (O’Brien et al., 2017). Our data suggest that the V1075 fauna lived after the end of the Aptian–Albian Cold Snap but prior to late Albian warming.

### 4.3 Constraining the influence of diagenesis

Multiple lines of evidence suggest that V1075 enamel preserves primary oxygen isotope compositions. First, we analyzed phosphate-bound oxygen which is more robust than carbonate bound oxygen, unless significant microbial alteration occurs, is the preferred phase to analyzed (Blake et al., 1998; Zazzo et al., 2004). Second,  $\delta^{18}\text{O}_p$  values between the sympatric V1075 taxonomic groups show expected magnitudes of offset (several‰ VSMOW) between aquatic, semi-aquatic, and fully terrestrial taxa. If the phosphate-bound oxygen had exchanged significantly with diagenetic fluids, we would expect homogenized  $\delta^{18}\text{O}_p$  values across the assemblage (Kohn and Cerling, 2002). Although it is possible that diagenesis may have caused a  $\delta^{18}\text{O}_p$  bulk shift

without homogenization, our reconstructed  $\delta^{18}\text{O}_{\text{sw}}$  values agree with other latitude-adjusted proxy data (Suarez et al., 2021), suggesting that any diagenetic bias in our data might be small (Suarez et al., 2014).

Third, we evaluated differential diagenetic influence between tissue types (i.e., dentine, bone, and enamel). Bone and dentine are more susceptible to diagenetic overprinting than enamel due to differences in crystallinity and porosity (Kohn and Cerling, 2002). We targeted pure enamel in our tooth samples; however, in teeth with thin enamel, it is likely that some dentine was inadvertently included in the drilled sample. We considered the possibility that variable degrees of dentine/enamel mixing during sampling may have been a significant factor behind the heterogeneous distribution of our  $\delta^{18}\text{O}_p$  data. We analyzed both dentine and enamel from one “Neosuchian G” tooth and found that the mean  $\delta^{18}\text{O}_p$  value of dentine ( $n = 2$ ) was  $\sim 1\%$  lower than that of enamel ( $n = 2$ ). If  $\delta^{18}\text{O}_p$  variability was strongly influenced by mixing isotopically distinct enamel and dentine during sampling, taxa with thin enamel would likely show greater intra-taxon  $\delta^{18}\text{O}_p$  variation than those with thick enamel, as samples from thin enamel often include some dentine. However, we observe similar standard errors in  $\delta^{18}\text{O}_p$  of both thick-enamel (Sauropoda and “Neosuchian B”) and thin-enamel taxa (Ornithischia, Maniraptora, “Neosuchian G,” “Neosuchian A”) in the V1075 assemblage (Table 1). V1075 bone phosphates may be slightly altered like dentine. Turtles, unlike other analyzed V1075 taxa, do not have teeth, and so bone is the only material

available. We targeted dense cortical bone in carapace fragments and avoided highly porous cancellous regions. Reconstructed  $\delta^{18}\text{O}_{\text{sw}}$  values between “Neosuchian G” tooth enamel and *Glyptops* bone are nearly identical, suggesting that both preserve similar signals.

Alteration of bone and dentine towards deep burial diagenetic values could explain the narrow distribution of turtle values near the overall mean. If dentine was more altered than enamel, dentine-enamel mixing in tooth samples might result in mixed samples clustering near a mean value, while pure enamel samples could deviate further, creating skewed distributions toward the overall mean for each taxon. This process would likely produce an overall normal distribution. However, the data do not fully support this hypothesis: the mean *Glyptops* value does not align with the overall mean, the distribution includes outliers and is not normal, and only two taxonomic groups exhibit non-normal distributions. This suggests that the data is not homogenized around a constrained  $\delta^{18}\text{O}$  as would be the case if bone oxygen had equilibrated with diagenetic fluids.

## 5 Future work

To understand variability of the Cloverly hydroclimate across space and time, spatial and temporal sampling coverage of multiple hydrological archives is required. The data presented here show that vertebrate bioapatite can serve as a component of that effort. Assessment of variability within and between fossil taxa presented in this study can now inform efficient multi-taxon isotopic sampling from a broad array of geographic and stratigraphic positions in the Cloverly. Additional broad scale multi-taxon studies utilizing oxygen and other isotope systems are needed to characterize mid-Cretaceous vertebrate faunas well enough that the isotopic niche structures and proxy reconstructions can be rigorously compared across space and time. However, there remains a paucity of multi-taxon traditional isotopic studies of Cretaceous terrestrial ecosystems.

In parallel with traditional approaches, emerging measurements such as  $\Delta^{17}\text{O}$  (triple oxygen isotopes) and  $\Delta_{47}-\Delta_{48}$  (dual clumped isotopes) may offer expanded insights. Recent advances in  $\Delta^{17}\text{O}$  (triple oxygen isotope) measurements hold promise for controlling for one of the major confounding factors on  $\delta^{18}\text{O}$  composition of continental vertebrates: evaporation.  $\Delta^{17}\text{O}$  is sensitive to evaporation but is not affected significantly by temperature (Passey et al., 2014; Aron et al., 2021; Passey and Levin, 2021). Thus, by evaluating the  $\Delta^{17}\text{O}$  of various taxa, we can differentiate between evaporative and brackish aquatic habitats, as well as between brackish and terrestrial habitats.

Our lack of evidence for diagenetic alteration of the V1075 fossils suggests that the Cloverly was not exposed to elevated burial temperatures and significant post-burial water-rock interactions. This encourages the use of  $\Delta_{47}$  (clumped isotopes) of Cloverly fossils to reconstruct both temperature and  $\delta^{18}\text{O}_{\text{sw}}$ . For example, Gray and Brandon (2025) recently presented a clumped isotope paleothermometer using the carbonate fraction of gar scales. Their proxy, calibrated on  $\Delta_{47}$  of modern gar scales and associated climate data, could provide an additional constraint on the temperature estimates we presented here using a multi-taxon  $\delta^{18}\text{O}_{\text{p}}$  approach.

Finally, future work should consider the development of models that incorporate key environmental and biological parameters influencing proxy reconstructions. Such aid in the interpretation of proxy values and help identify variables that can be further constrained.

## 6 Conclusion

We measured  $\delta^{18}\text{O}_{\text{phosphate}}$  of over 100 fossil individuals of multiple taxa from a single Albian nonmarine vertebrate microfossil bonebed in the Lower Cretaceous Cloverly Formation. Our data suggest that primary oxygen isotope signals are preserved in Cloverly vertebrate phosphates. For most of the analyzed taxa, we were able to distinguish aquatic and terrestrial habits. “Neosuchian B” (cf. Bernissartiidae) showed  $\delta^{18}\text{O}_{\text{p}}$  more consistent with sympatric terrestrial taxa than aquatic taxa. We interpret this as the result of these animals having spent significant amounts of time in brackish water or evaporatively enriched lake or pond waters. We reconstructed  $\delta^{18}\text{O}_{\text{sw}}$  from each turtle and crocodylomorph taxon and used this data to examine the paleohydrologic landscape that the V1075 fauna lived in. We estimate a warm season  $\delta^{18}\text{O}_{\text{sw}}$  of  $-7.9\text{‰}$  (95% CI:  $-10.0$ ,  $-5.6\text{‰}$ ), which is consistent with other vertebrate phosphate derived estimates from the mid Cretaceous Western Interior. We combined this  $\delta^{18}\text{O}_{\text{sw}}$  estimate with  $\delta^{18}\text{O}_{\text{p}}$  of gar to reconstruct a mean annual warm season air temperature of  $26^{\circ}\text{C}$  (95% CI:  $9$ ,  $43^{\circ}\text{C}$ ). This temperature estimate is consistent with other mid-Cretaceous estimates and with model predictions at this paleolatitude. While our quantitative temperature estimates are subject to substantial uncertainty, primarily stemming from  $\delta^{18}\text{O}_{\text{sw}}$  reconstructions and regression model parameters, these uncertainties primarily affect the precision of our values rather than the overall interpretation, which robustly supports a seasonally warm climate consistent with other mid-Cretaceous reconstructions. Our temperature estimate suggests that the Aptian-Albian Cold Snap had ended by the time the V1075 fauna was alive, but that temperatures were still much cooler than in the following Cretaceous Thermal Maximum. Similar studies from multiple sites in the Cloverly and the application of triple oxygen and clumped isotopes will help reconstruct spatial and temporal patterns in climate and evolution.

## Data availability statement

The original contributions presented in the study are publicly available. This data can be found here: <https://doi.org/10.60520/IEDA/113456>.

## Author contributions

MA: Conceptualization, Data curation, Formal Analysis, Investigation, Methodology, Project administration, Visualization, Writing – original draft, Writing – review and editing. MS: Conceptualization, Funding acquisition, Methodology, Project administration, Validation, Writing – review and editing. TA: Conceptualization, Validation, Writing – review and editing. CS:

Conceptualization, Funding acquisition, Methodology, Supervision, Validation, Writing – review and editing.

## Funding

The author(s) declare that financial support was received for the research and/or publication of this article. This work was largely funded by National Science Foundation award # EAR1925942. Additional funding was also provided by the University of Kansas Department of Geology.

## Acknowledgments

We would like to thank the Vertebrate Paleontology staff at the University of Oklahoma Sam Noble Museum of Natural History for making these fossils available for study, especially Jen Larsen and Kyle Davies. We acknowledge Bruce Barnett for stable isotope analyses. We also thank Noah McLean for help with statistical modeling, Mike D'Emic for a helpful discussion on archosaur tooth growth, and Bryan Rodriguez-Colon for help with sample preparation. Generative AI technology (ChatGPT, GPT-4, OpenAI) was used to assist in drafting, editing, and refining portions of the manuscript. It was also employed in the design and generation of R code for statistical analyses and data visualization. All AI-generated content was thoroughly reviewed and edited by the authors to ensure accuracy and integrity.

## Conflict of interest

The authors declare that the research was conducted in the absence of any commercial or financial relationships that could be construed as a potential conflict of interest.

## References

- Adams, T. L. (2015). Small crocodyliform from the lower cretaceous (late aptian) of central Texas and its systematic relationship to the evolution of eusuchia. *J. Paleontology* 88, 1031–1049. doi:10.1666/12-089
- Amiot, R., Buffetaut, E., Lécuyer, C., Escarguel, G., Fluteau, F., and Martineau, F. (2006). Oxygen isotopes from biogenic apatites suggest widespread endothermy in Cretaceous dinosaurs. *Earth Planet. Sci. Lett.* 246, 41–54. doi:10.1016/j.epsl.2006.04.018
- Amiot, R., Buffetaut, E., Lécuyer, C., Fernandez, V., Fourrel, F., Martineau, F., et al. (2009). Oxygen isotope composition of continental vertebrate apatites from Mesozoic formations of Thailand; environmental and ecological significance. *Geol. Soc. Lond. Spec. Publ.* 315, 271–283. doi:10.1144/sp315.19
- Amiot, R., Kusuhashi, N., Saegusa, H., Shibata, M., Ikegami, N., Shimojima, S., et al. (2021). Paleoclimate and ecology of Cretaceous continental ecosystems of Japan inferred from the stable oxygen and carbon isotope compositions of vertebrate bioapatite. *J. Asian Earth Sci.* 205, 104602. doi:10.1016/j.jseas.2020.104602
- Amiot, R., Lécuyer, C., Escarguel, G., Billon-Bruyat, J. P., Buffetaut, E., Fourrel, F., et al. (2007). Oxygen isotope fractionation between crocodylian phosphate and water. *Palaeogeogr. Palaeoclimatol. Palaeoecol.* 243 (3–4), 412–420. doi:10.1016/j.palaeo.2006.08.013
- Amiot, R., Wang, X., Lécuyer, C., Buffetaut, E., Boudad, L., Cavin, L., et al. (2010). Oxygen and carbon isotope compositions of middle Cretaceous vertebrates from North Africa and Brazil: ecological and environmental significance. *Palaeogeogr. Palaeoclimatol. Palaeoecol.* 297, 439–451. doi:10.1016/j.palaeo.2010.08.027
- Amiot, R., Wang, X., Zhou, Z., Wang, X., Buffetaut, E., Lécuyer, C., et al. (2011). Oxygen isotopes of East Asian dinosaurs reveal exceptionally cold Early Cretaceous climates. *Proc. Natl. Acad. Sci. U. S. A.* 108, 5179–5183. doi:10.1073/pnas.1011369108
- Amiot, R., Wang, X., Zhou, Z., Wang, X., Lécuyer, C., Buffetaut, E., et al. (2015). Environment and ecology of East Asian dinosaurs during the Early Cretaceous inferred from stable oxygen and carbon isotopes in apatite. *J. Asian Earth Sci.* 98, 358–370. doi:10.1016/j.jseas.2014.11.032
- Andrzejewski, K., and Tabor, N. J. (2020). Paleoenvironmental and paleoclimatic reconstruction of Cretaceous (Aptian–Cenomanian) terrestrial formations of Texas and Oklahoma using phyllosilicates. *Palaeogeogr. Palaeoclimatol. Palaeoecol.* 543, 109491. doi:10.1016/j.palaeo.2019.109491
- Aron, P. G., Levin, N. E., Beverly, E. J., Huth, T. E., Passey, B. H., Pelletier, E. M., et al. (2021). Triple oxygen isotopes in the water cycle. *Chem. Geol.* 565, 120026. doi:10.1016/j.chemgeo.2020.120026
- Barrick, R. E., Fischer, A. G., and Showers, W. J. (1999). Oxygen isotopes from turtle bone: applications for terrestrial paleoclimates? *Palaio* 14, 186. doi:10.2307/3515374
- Barron, E. J. (1983). A warm, equable Cretaceous: the nature of the problem. *Earth-Science Rev.* 19, 305–338. doi:10.1016/0012-8252(83)90001-6
- Blake, R. E., O'Neil, J. R., and Garcia, G. A. (1998). Effects of microbial activity on the  $\delta^{18}\text{O}$  of dissolved inorganic phosphate and textural features of synthetic apatites. *Am. Mineralogist* 83 (11–12), 1516–1531. doi:10.2138/am-1998-11-1240
- Breecker, D. O., Sharp, Z. D., and McFadden, L. D. (2009). Seasonal bias in the formation and stable isotopic composition of pedogenic carbonate in modern soils

## Publisher's note

All claims expressed in this article are solely those of the authors and do not necessarily represent those of their affiliated organizations, or those of the publisher, the editors and the reviewers. Any product that may be evaluated in this article, or claim that may be made by its manufacturer, is not guaranteed or endorsed by the publisher.

## Supplementary material

The Supplementary Material for this article can be found online at: <https://www.frontiersin.org/articles/10.3389/feart.2025.1497416/full#supplementary-material>

### Supplementary Data Sheet 1 |

Raw isotopic and analytical data for vertebrate phosphate samples from the Cloverly Formation used in this study. Includes specimen identifiers, taxonomic assignment, sample metadata, analytical yield information, and  $\delta^{18}\text{O}$  (VSMOW) values for bioapatite. Data are organized by specimen and sample ID, with tissue type and element descriptions provided for each entry.

### Supplementary Data Sheet 2 |

R Markdown HTML output detailing data processing, model fitting, and Monte Carlo simulations used to estimate paleoenvironmental parameters from  $\delta^{18}\text{O}$  values in vertebrate phosphate. This report includes all code, summary results, and figures generated from the Frontiers\_V1075\_Project RStudio project. A link to the GitHub repository containing all data and code used in this study is provided within the report.

### Supplementary Data Sheet 3 |

This document provides a detailed Standard Operating Procedure (SOP) for precipitating silver phosphate ( $\text{Ag}_3\text{PO}_4$ ) from bioapatite for oxygen isotope analysis. The protocol follows the methods of O'Neil (1994) and Vennemann et al. (2002), with additional annotations by Damon Basset and Celina Suarez. It includes step-by-step instructions for sample preparation, chemical treatments (acetone rinse, bleaching, precipitation steps), and final  $\text{Ag}_3\text{PO}_4$  recovery. It also provides instructions for preparing key reagents, including silver amine solution, NaOCl, KOH, and KF, with complete molarity calculations. This SOP was used for all samples analyzed in the present study.

- from central New Mexico, USA. *Geol. Soc. Am. Bull.* 121, 630–640. doi:10.1130/B26413.1
- Buffetaut, E., and Ford, R. L. E. (1979). The crocodylian *Bernissartia* in the wealden of the Isle of Wight. *Palaeontology* 22, 905–912.
- Burgener, L., Hyland, E., Huntington, K. W., Sheldon, N. D., Hoke, G. D., and Schauer, A. D. (2019). Revisiting the equable climate problem during the Late Cretaceous greenhouse using paleosol carbonate clumped isotope temperatures from the Campanian of the Western Interior Basin, USA. *Palaeogeogr. Palaeoclimatol. Palaeoecol.* 516, 244–267. doi:10.1016/j.palaeo.2018.12.004
- Burgener, L. K., Huntington, K. W., Hoke, G. D., Schauer, A. D., Ringham, M. C., Latorre, C., et al. (2016). Variations in soil carbonate formation and seasonal bias over >4 km of relief in the western Andes (30°S) revealed by clumped isotope thermometry. *Earth Planet. Sci. Lett.* 441, 188–199. doi:10.1016/j.epsl.2016.02.033
- Carrano, M. T., Oreska, M. P. J., Murch, A., Trujillo, K. C., and Chamberlain, K. R. (2022). Vertebrate paleontology of the Cloverly Formation (Lower Cretaceous), III: a new species of *Albanerpeton*, with biogeographic and paleoecological implications. *J. Vertebrate Paleontology* 41 (5), e2003372. doi:10.1080/02724634.2021.2003372
- Cerling, T. E., and Sharp, Z. D. (1996). Stable carbon and oxygen isotope analysis of fossil tooth enamel using laser ablation. *Palaeogeogr. Palaeoclimatol. Palaeoecol.* 126, 173–186. doi:10.1016/S0031-0182(96)00078-8
- Cifelli, R. L. (1999). Tribosphenic mammal from the North American early cretaceous. *Nature* 401, 363–366. doi:10.1038/43860
- Cifelli, R. L., Gardner, J. D., Nydam, R. L., and Brinkman, D. L. (1999). Additions to the vertebrate fauna of the Antlers formation (lower cretaceous). *Southeast. Okla. Okla. Geol. Notes.* 57, 124–131.
- Cifelli, R. L., Wible, J. R., and Jenkins, F. A. (1998). Triconodont mammals from the Cloverly Formation (lower cretaceous), Montana and Wyoming. *J. Vertebrate Paleontology* 18, 237–241. doi:10.1080/02724634.1998.10011048
- Cullen, T. M., Longstaffe, F. J., Wortmann, U. G., Huang, L., Fanti, F., Goodwin, M. B., et al. (2020). Large-scale stable isotope characterization of a Late Cretaceous dinosaur-dominated ecosystem. *Geology* 48, 546–551. doi:10.1130/g47399.1
- Cullen, T. M., Zhang, S., Spencer, J., Cousens, B., and Button, D. (2022). Sr-O-C isotope signatures reveal herbivore niche-partitioning in a Cretaceous ecosystem. *Palaeontology* 65. doi:10.1111/pala.12591
- DeCelles, P. G. (2004). Late Jurassic to Eocene evolution of the Cordilleran thrust belt and foreland basin system, western U.S.A. *Am. J. Sci.* 304, 105–168. doi:10.2475/ajs.304.2.105
- D’Emic, M. D., Foreman, B. Z., Jud, N. A., Britt, B. B., Schmitz, M., and Crowley, J. L. (2019). Chronostratigraphic Revision of the Cloverly Formation (Lower Cretaceous, Western Interior, USA). *Bull. Peabody Mus. Nat. Hist.* 60, 3–40. doi:10.3374/014.060.0101
- Elliott, W. S., Suttner, L. J., and Pratt, L. M. (2007). Tectonically induced climate and its control on the distribution of depositional systems in a continental foreland basin, Cloverly and Lakota Formations (Lower Cretaceous) of Wyoming, U.S.A. *Sediment. Geol.* 202, 730–753. doi:10.1016/j.sedgeo.2007.09.001
- Evers, S. W. (2023). Mandibular anatomy of the paracryptidire *Glyptops ornatus* supports active hunting behavior in a Jurassic turtle. *Anatomical Rec.* 307 (6), 2007–2017. doi:10.1002/ar.25320
- Fricke, H. C., and Wing, S. L. (2004). Oxygen isotope and paleobotanical estimates of temperature and  $\delta^{18}\text{O}$ -latitude gradients over North America during the early Eocene. *Am. J. Sci.* 304 (7), 612–635. doi:10.2475/ajs.304.7.612
- Gardner, J. (1999). The amphibian *Albanerpeton arthridion* and the Aptian–Albian biogeography of albanerpetontids. *Palaeontology* 42, 529–544. doi:10.1111/1475-4983.00083
- Gray, K. E., and Brandon, M. T. (2025). A terrestrial thermometer using carbonate clumped isotopes from gas scales. *Geochem. Geophys. Geosystems* 26 (2), e2024GC011714. doi:10.1029/2024GC011714
- Grossman, E. L., and Joachimski, M. M. (2022). Ocean temperatures through the Phanerozoic reassessed. *Sci. Rep.* 12, 8938. doi:10.1038/s41598-022-11493-1
- Harper, D. T., Suarez, M. B., Uglesich, J., You, H., Li, D., and Dodson, P. (2021). Aptian–Albian clumped isotopes from northwest China: cool temperatures, variable atmospheric  $p\text{CO}_2$  and regional shifts in the hydrologic cycle. *Clim. Past* 17, 1607–1625. doi:10.5194/cp-17-1607-2021
- Heller, A., Angevine, C. L., Winslow, N. S., and Paola, C. (1988). Two-phase stratigraphic model of foreland-basin sequences. *Geology* 16, 501–504. doi:10.1130/0091-7613(1988)016<0501:tpsmof>2.3.co;2
- Hren, M. T., and Sheldon, N. D. (2012). Temporal variations in lake water temperature: Paleoenvironmental implications of lake carbonate  $\delta^{18}\text{O}$  and lake temperature models. *Palaeogeogr. Palaeoclimatol. Palaeoecol.* 337–338, 81–90. doi:10.1016/j.palaeo.2012.03.020
- Huber, B. T., Macleod, K. G., Watkins, D. K., and Coffin, M. F. (2018). The rise and fall of the Cretaceous Hot Greenhouse climate. *Glob. Planet. Change* 167, 1–23. doi:10.1016/j.gloplacha.2018.04.004
- Huth, T. E., Cerling, T. E., Marchetti, D. W., Bowling, D. R., Ellwein, A. L., and Passet, B. H. (2019). Seasonal bias in soil carbonate formation and its implications for interpreting high-resolution paleoarchives: Evidence from southern Utah. *J. Geophys. Res. Biogeosciences* 124 (3), 616–632. doi:10.1029/2018JG004496
- Jenkins, J. F., and Schaff, C. R. (1988). The Early Cretaceous mammal *Gobiconodon* (Mammalia, Triconodonta) from the Cloverly Formation in Montana. *J. Vertebrate Paleontology* 8, 1–24. doi:10.1080/02724634.1988.10011681
- Jones, M. M., Petersen, S. V., and Curley, A. N. (2022). A tropically hot mid-Cretaceous North American Western Interior Seaway. *Geology* 50, 954–958. doi:10.1130/g49998.1
- Joyce, W. G. (2017). A Review of the Fossil Record of Basal Mesozoic Turtles. *Bull. Peabody Mus. Nat. Hist.* 58, 65–113. doi:10.3374/014.058.0105
- Joyce, W. G., Sterli, J., and Chapman, S. D. (2015). The skeletal morphology of the solemydid turtle *Naomichelys speciosa* from the Early Cretaceous of Texas. *J. Paleontology* 88, 1257–1287. doi:10.1666/14-002
- Judd, E. J., Tierney, J. E., Lunt, D. J., Montañez, I. P., Huber, B. T., Wing, S. L., et al. (2024). A 485-million-year history of Earth’s surface temperature. *Science* 385 (6715), eadk3705. doi:10.1126/science.adk3705
- Kelson, J. R., Huntington, K. W., Breecker, D. O., Burgener, L. K., Gallagher, T. M., Hoke, G. D., et al. (2020). A proxy for all seasons? A synthesis of clumped isotope data from Holocene soil carbonates. *Quat. Sci. Rev.* 234, 106259. doi:10.1016/j.quascirev.2020.106259
- Koch, P. L. (2007). “Isotopic study of the biology of modern and fossil vertebrates,” in *Stable isotopes in ecology and environmental science*. Editors R. Michener, and K. Lajtha 2nd ed. (Malden, MA: Blackwell Publishing), 99–154.
- Kohn, M. J. (1996). Predicting animal  $\delta^{18}\text{O}$ : Accounting for diet and physiological adaptation. *Geochimica Cosmochimica Acta* 60 (23), 4811–4829. doi:10.1016/S0016-7037(96)00240-2
- Kohn, M. J., and Cerling, T. E. (2002). Stable Isotope Compositions of Biological Apatite. *Rev. Mineral. Geochem.* 48, 455–488. doi:10.2138/rmg.2002.48.12
- Kolodny, Y., Luz, B., and Navon, O. (1983). Oxygen isotope variations in phosphate of biogenic apatites, I. Fish bone apatite—rechecking the rules of the game. *Earth Planet. Sci. Lett.* 64, 398–404. doi:10.1016/0012-821X(83)90100-0
- Lee–Thorp, J. (2002). Two decades of progress towards understanding fossilization processes and isotopic signals in calcified tissue minerals. *Archaeometry* 44, 435–446. doi:10.1111/1475-4754.t01-1-00076
- Longinelli, A. (1966). Ratios of oxygen-18:oxygen-16 in phosphate and carbonate from living and fossil marine organisms. *Nature* 211, 923–927. doi:10.1038/211923a0
- Longinelli, A., and Nuti, S. (1973a). Revised phosphate-water isotopic temperature scale. *Earth Planet. Sci. Lett.* 19 (3), 373–376. doi:10.1016/0012-821X(73)90088-5
- Longinelli, A., and Nuti, S. (1973b). Oxygen isotope measurements of phosphate from fish teeth and bones. *Earth Planet. Sci. Lett.* 20 (3), 337–340. doi:10.1016/0012-821X(73)90007-1
- Ludvigson, G. A., Joeckel, R. M., Murphy, L. R., Stockli, D. F., González, L. A., Suarez, C. A., et al. (2015). The emerging terrestrial record of Aptian–Albian global change. *Cretac. Res.* 56, 1–24. doi:10.1016/j.cretres.2014.11.008
- Martin, J. E., Delfino, M., and Smith, T. (2020). Osteology and phylogenetic position of *Bernissartia fagesii*, a neosuchian crocodyliform from the Early Cretaceous of Europe. *J. Vertebrate Paleontology* 40 (3), e1780601. doi:10.1080/02724634.2020.1780601
- Maxwell, W. D., and Horner, J. R. (1994). Neonate dinosaurian remains and dinosaurian eggshell from the Cloverly Formation, Montana. *J. Vertebrate Paleontology* 14, 143–146. doi:10.1080/02724634.1994.10011547
- McAnena, A., Flögel, S., Hofmann, P., Herrle, J. O., Griesand, A., Pross, J., et al. (2013). Atlantic cooling associated with a marine biotic crisis during the mid-Cretaceous period. *Nat. Geosci.* 6, 558–561. doi:10.1038/ng1850
- McCurry, M. R., Evans, A. R., Fitzgerald, E. M. G., Mchenry, C. R., Bevirt, J., and Pyenson, N. D. (2019). The repeated evolution of dental apicobasal ridges in aquatic-feeding mammals and reptiles. *Biol. J. Linn. Soc.* 127, 245–259. doi:10.1093/biolinnean/blz025
- Moberly, R. (1960). Morrison, Cloverly, and Sykes Mountain Formations, Northern Bighorn Basin, Wyoming and Montana. *Bull. Geol. Soc. Am.* 71, 1137–1176. doi:10.1130/0016-7606(1960)71[1137:mcsmf]2.0.co;2
- Montefeltro, F. C., Larsson, H. C., De Franca, M. A., and Langer, M. C. (2013). A new neosuchian with Asian affinities from the Jurassic of northeastern Brazil. *Naturwissenschaften* 100, 835–841. doi:10.1007/s00114-013-1083-9
- Neubauer, P., and Andersen, K. H. (2019). Thermal performance of fish is explained by an interplay between physiology, behaviour, and ecology. *Conserv. Physiol.* 7 (1), coz025. doi:10.1093/conphys/coz025
- Nydam, R. L., and Cifelli, R. L. (2002). A new teiid lizard from the Cedar Mountain Formation (Albian–Cenomanian boundary) of Utah. *J. Vertebrate Paleontology* 22, 276–285. doi:10.1671/0272-4634(2002)022[0276:Antlft]2.0.co;2
- O’Brien, C. L., Robinson, S. A., Pancost, R. D., Sinningh Damsté, J. S., Schouten, S., Lunt, D. J., et al. (2017). Cretaceous sea-surface temperature evolution: Constraints from TEX86 and planktonic foraminiferal oxygen isotopes. *Earth-Science Rev.* 172, 224–247. doi:10.1016/j.earscirev.2017.07.012

- Orchard, C. (2024). *Nonmarine stratigraphic architecture in response to transgression: a test in the Cretaceous Cloverly Formation of Wyoming*. M.S. thesis (Athens, Georgia: University of Georgia).
- Oreska, M. P. J., Carrano, M. T., and Dzikiewicz, K. M. (2013). Vertebrate paleontology of the Cloverly Formation (Lower Cretaceous), I: faunal composition, biogeographic relationships, and sampling. *Journal Vertebrate Paleontology* 33, 264–292. doi:10.1080/02724634.2012.717567
- Ostrom, J. H. (1970). "Stratigraphy and paleontology of the Cloverly Formation (Lower Cretaceous) of the Bighorn Basin area, Wyoming and Montana," in *Peabody Museum of natural history* (New Haven: Yale University), 234.
- Passey, B. H., Hu, H., Ji, H., Montanari, S., Li, S., Henkes, G. A., et al. (2014). Triple oxygen isotopes in biogenic and sedimentary carbonates. *Geochimica Cosmochimica Acta* 141, 1–25. doi:10.1016/j.gca.2014.06.006
- Passey, B. H., and Levin, N. E. (2021). Triple Oxygen Isotopes in Meteoric Waters, Carbonates, and Biological Apatites: Implications for Continental Paleoclimate Reconstruction. *Rev. Mineralogy Geochem.* 86, 429–462. doi:10.2138/rmg.2021.86.13
- Peters, N. A., Huntington, K. W., and Hoke, G. D. (2013). Hot or not? Impact of seasonally variable soil carbonate formation on paleotemperature and O-isotope records from clumped isotope thermometry. *Earth Planet. Sci. Lett.* 361, 208–218. doi:10.1016/j.epsl.2012.10.024
- Pouech, J., Amiot, R., Lécuyer, C., Mazin, J. M., Martineau, F., and Fourel, F. (2014). Oxygen isotope composition of vertebrate phosphates from Cherves-de-Cognac (Berriasian, France): Environmental and ecological significance. *Palaeogeogr. Palaeoclimatol. Palaeoecol.* 410, 290–299. doi:10.1016/j.palaeo.2014.05.036
- Puceat, E., Lécuyer, C., Sheppard, S. M. F., Dera, G., Martineau, F., Bardet, N., et al. (2010). Revised phosphate–water fractionation equation reassessing paleotemperatures derived from biogenic apatite. *Earth. Plane. Sci. Lett.* 298, 135–142. doi:10.1016/j.epsl.2010.07.034
- Rodríguez-López, J. P., Liesa, C. L., Pardo, G., Meléndez, N., Soria, A. R., and Skilling, I. (2016). Glacial dropstones in the western Tethys during the late Aptian–early Albian cold snap: Palaeoclimate and palaeogeographic implications for the mid-Cretaceous. *Palaeogeogr. Palaeoclimatol. Palaeoecol.* 452, 11–27. doi:10.1016/j.palaeo.2016.04.004
- Rogers, R. R., and Brady, M. E. (2010). Origins of microfossil bonebeds: Insights from the Upper Cretaceous Judith River Formation of north-central Montana. *PALAIOS* 25 (6), 409–424. doi:10.2110/palo.2009.p09-138r
- Rogers, R. R., Eberth, D. A., and Fiorillo, A. R. (2007). in *Bonebeds: genesis, analysis, and paleobiological significance* (Chicago: University of Chicago Press), 499.
- Rozanski, K., Araguás-Araguás, L., and Gonfiantini, R. (1993). Isotopic patterns in modern global precipitation. *Am. Geophys. Union, Geophys. Monogr.* 78, 1–36. doi:10.1029/GM078p0001
- Scotese, C. R. (2021). An atlas of Phanerozoic paleogeographic maps: The seas come in and the seas go out. *Annu. Rev. Earth Planet. Sci.* 49, 679–728. doi:10.1146/annurev-earth-081320-064052
- Scotese, C. R., Vérard, C., Burgener, L., Elling, R. P., and Kocsis, A. T. (2025). The Cretaceous world: plate tectonics, palaeogeography and palaeoclimate. *Geol. Soc. Lond. Spec. Publ.* 544, 31–202. doi:10.1144/SP544-2024-28
- Spagna, P., Gomez, B., and Daviero-Gomez, V. (2012). Local-scale analysis of plant community from the Early Cretaceous riparian ecosystem of Hautrage, Belgium. *Palaeogeogr. Palaeoclimatol. Palaeoecol.* 361–362, 208–218. doi:10.1016/j.palaeo.2012.10.024
- Suarez, C. A., Frucci, M. N., Tompkins, T. B., and Suarez, M. B. (2021). Quantification of a North American greenhouse hydrological cycle: using oxygen isotopic composition of phosphate from Early Cretaceous (Aptian–Albian) turtles. *Geol. Soc. Lond. Spec. Publ.* 507, 335–345. doi:10.1144/SP507-2020-90
- Suarez, C. A., González, L. A., Ludvigson, G. A., Cifelli, R. L., and Tremain, E. (2012). Water utilization of the Cretaceous Mussentuchit Member local vertebrate fauna, Cedar Mountain Formation, Utah, USA: Using oxygen isotopic composition of phosphate. *Palaeogeogr. Palaeoclimatol. Palaeoecol.* 313–314. doi:10.1016/j.palaeo.2011.10.011
- Suarez, C. A., Gonzalez, L. A., Ludvigson, G. A., Kirkland, J. I., Cifelli, R. L., and Kohn, M. J. (2014). Multi-Taxa Isotopic Investigation of Paleohydrology In the Lower Cretaceous Cedar Mountain Formation, Eastern Utah, U.S.A.: Deciphering Effects Of the Nevadaplano Plateau On Regional Climate. *J. Sediment. Res.* 84, 975–987. doi:10.2110/jsr.2014.76
- Suarez, M. B., González, L. A., and Ludvigson, G. A. (2011). Quantification of a greenhouse hydrologic cycle from equatorial to polar latitudes: The mid-Cretaceous water bearer revisited. *Palaeogeogr. Palaeoclimatol. Palaeoecol.* 307, 301–312. doi:10.1016/j.palaeo.2011.05.027
- Suarez, M. B., Knight, J. A., Godet, A., Ludvigson, G. A., Snell, K. E., Murphy, L., et al. (2021). Multiproxy strategy for determining palaeoclimate parameters in the Ruby Ranch Member of the Cedar Mountain Formation. *Geol. Soc. Lond. Spec. Publ.* 507, 313–334. doi:10.1144/sp507-2020-85
- Sweetman, S. C., Goedert, J., and Martill, D. M. (2014). A preliminary account of the fishes of the Lower Cretaceous Wessex Formation (Wealden Group, Barremian) of the Isle of Wight, southern England. *Biol. J. Linn. Soc.* 113, 872–896. doi:10.1111/bij.12369
- Tennant, J. P., Mannion, P. D., and Upchurch, P. (2016). Evolutionary relationships and systematics of Atoposauridae (Crocodylomorpha: Neosuchia): implications for the rise of Eusuchia. *Zoological J. Linn. Soc.* 177, 854–936. doi:10.1111/zooj.12400
- Ufnar, D. F., Gonzalez, L. A., Ludvigson, G. A., Brenner, R. L., and Witzke, B. J. (2002). The mid-Cretaceous water bearer: isotope mass balance quantification of the Albian hydrologic cycle. *Palaeogeogr. Palaeoclimatol. Palaeoecol.* 188, 51–71. doi:10.1016/s0031-0182(02)00530-8
- Ullmann, P. V., Varricchio, D., and Knell, M. J. (2011). Taphonomy and taxonomy of a vertebrate microsite in the mid-Cretaceous (Albian–Cenomanian) Blackleaf Formation, southwest Montana. *Hist. Biol.* 24, 1–18. doi:10.1080/08912963.2011.602405
- Vaes, B., van Hinsbergen, D. J. J., and Spakman, W. (2023). A global apparent polar wander path for the last 320 Ma calculated from site-level paleomagnetic data. *Earth-Science Rev.* 235, 104547. doi:10.1016/j.earscirev.2023.104547
- van Hinsbergen, D. J. J., de Groot, L. V., van Schaik, S. J., Spakman, W., Bijl, P. K., Sluijs, A., et al. (2015). A paleolatitude calculator for paleoclimate studies. *PLOS ONE* 10 (6), e0126946. doi:10.1371/journal.pone.0126946
- Vennemann, T. W., Fricke, H. C., Blake, R. E., O'Neil, J. R., and Colman, A. (2002). Oxygen isotope analysis of phosphates: a comparison of techniques for analysis of Ag<sub>3</sub>PO<sub>4</sub>. *Chem. Geol.* 185, 321–336. doi:10.1016/s0009-2541(01)00413-2
- Wilberg, E. W., Turner, A. H., and Brochu, C. A. (2019). Evolutionary structure and timing of major habitat shifts in Crocodylomorpha. *Sci. Rep.* 9, 514. doi:10.1038/s41598-018-36795-1
- Winkler, D. A., Murry, P. A., and Jacobs, L. L. (1990). Early Cretaceous (Comanchean) vertebrates of central Texas. *J. Vertebrate Paleontology* 10, 95–116. doi:10.1080/02724634.1990.10011794
- Zazzo, A., Lécuyer, C., Sheppard, S. M. F., Grandjean, P., and Mariotti, A. (2004). Diagenesis and the reconstruction of paleoenvironments: A method to restore original  $\delta^{18}\text{O}$  values of carbonate and phosphate from fossil tooth enamel. *Geochimica Cosmochimica Acta* 68 (10), 2245–2258. doi:10.1016/j.gca.2003.11.009
- Zhou, J., Poulsen, C. J., Pollard, D., and White, T. S. (2008). Simulation of modern and middle Cretaceous marine  $\delta^{18}\text{O}$  with an ocean–atmosphere general circulation model. *Paleoceanography* 23, PA3223. doi:10.1029/2008PA001596